ORIGINAL ARTICLE

Tumour-associated CD204$^+$ microglia/macrophages accumulate in perivascular and perinecrotic niches and correlate with an interleukin-6-enriched inflammatory profile in glioblastoma

Mia D. Sørensen[1,2] | Bjarne W. Kristensen[1,2,3,4]

[1]Department of Pathology, Odense University Hospital, Odense, Denmark

[2]Department of Clinical Research, University of Southern Denmark, Odense, Denmark

[3]Department of Pathology, Rigshospitalet, Copenhagen University Hospital, Copenhagen, Denmark

[4]Department of Clinical Medicine and Biotech Research and Innovation Center (BRIC), University of Copenhagen, Copenhagen, Denmark

Correspondence

Mia D. Sørensen, Department of Pathology, Odense University Hospital, J. B. Winsloews Vej 15, 5000. Odense C, Denmark.
Email: mia.soerensen@rsyd.dk

Abstract

Aims: Glioblastomas are heterogeneous tumours with a rich tumour microenvironment particularly comprised of tumour-associated microglia/macrophages (TAMs), but also containing a population of dedifferentiated/stem-like glioblastoma cells. Both cell populations contribute to tumour aggressiveness and immune evasion through the actions of various signalling molecules. The scavenger and pattern recognition receptor CD204 is associated with a pro-tumourigenic phenotype of TAMs and has a negative prognostic value. Our objective was to investigate the possible interaction between TAMs and dedifferentiated glioblastoma cells and characterise the myeloid phenotype of CD204-enriched glioblastomas.

Methods: Double immunohistochemistry and cell counting was performed on eight glioblastoma samples to estimate the expression and interaction level between dedifferentiated/stem-like tumour cells and TAMs. Using the NanoString technology, myeloid transcriptome profiling was performed on 46 glioblastomas, which had been selected based on their protein expression levels of CD204 and ionised calcium-binding adaptor molecule-1 (IBA1). The results were validated by immunohistochemistry and *in silico* gene expression analyses.

Results: TAMs especially CD204$^+$ TAMs accumulated in perivascular and perinecrotic niches in close proximity to podoplanin$^+$ glioblastoma cells. Gene profiling revealed that CD204-enriched glioblastoma has a unique signature with upregulation of genes related to hypoxia, angiogenesis and invasion, including interleukin-6. The gene signature favoured a poor prognosis in patients with glioblastoma.

Conclusions: This is the first study to characterise the role of CD204 in the myeloid microenvironment of glioblastoma. Our results support the unfavourable prognostic impact of CD204 and suggest that CD204 and interleukin-6 could serve as targets for re-education of TAMs and potentiation of current anti-glioma therapy.

KEYWORDS

CD204, glioblastoma, immunotherapy, interleukin-6, macrophage, microglia, nanostring, tumour microenvironment

INTRODUCTION

Glioblastoma, World Health Organization (WHO) Grade IV, is the most frequent and lethal primary brain tumour in adults accounting for almost 50% of all primary malignant brain neoplasms [1, 2]. Despite standard-of-care with surgery and adjuvant radio-chemotherapy [3], the prognosis is dismal with only 5% to 10% of patients alive at 5 years [2, 4]. Glioblastomas are highly invasive in nature and exhibit great intra- [5, 6] and inter-tumoural heterogeneity [7–9]. The heterogeneous tumour landscape is a result of both intrinsic [6, 8, 9] and extrinsic factors including the tumour microenvironment (TME) [10–13] and is believed to contribute to the inefficient treatment response, ultimately resulting in poor patient outcome [14–16]. Treatment resistance is partly due to tumour cell plasticity allowing glioblastoma cells to dedifferentiate to a stem cell-like state. Reportedly, cancer cells expressing markers related to a stem-like phenotype (e.g., CD133, CD44, and nestin) represent a population of cells which is highly proliferative, aggressive, and resistant towards radiation, as well as anti-angiogenic and chemotherapeutic agents [16–19]. These dedifferentiated cancer cells often reside and thrive in perivascular [20–22] and necrotic/hypoxic [20, 23] niches, closely interacting with several non-neoplastic cell types in the TME including endothelial cells and immune cells [11, 18, 24–27] that favour an immunosuppressive TME [28, 29].

In recent years, the interest in targeting the TME, especially the tumour immune microenvironment, has increased as a means to enhance the efficacy of anti-cancer therapies [9]. The immune cell landscape in cancer including brain tumours is highly diverse adding to the overall complexity of the tumour biology, and the composition of the immune infiltrate has been reported to predict response to immunotherapy including immune checkpoint inhibitors [13, 30]. Tumour-associated microglia and macrophages (TAMs) are the dominant immune cell population in gliomas [31], comprising up to 30% of the cellular content of glioblastomas [10, 32, 33]. Resident brain microglia and infiltrating peripheral macrophages are recruited and polarised towards a tumour-supportive phenotype by a variety of tumour-derived signalling molecules including colony-stimulating factor 1 (CSF1), (C-C motif) ligand 2 (CCL2), (C-X-C motif) ligand 3 (CXCL3), and interleukin-6 (IL6) [10, 33–35]. Increasing evidence suggests that TAMs are a mixed cell population taking on several phenotypes along the M1-M2 spectrum [32, 36–38], including the more undifferentiated M0 phenotype [39]. Single-cell RNA sequencing of TAMs has shown that pro-inflammatory M1 and anti-inflammatory M2 genes are co-expressed at a cellular level [40].

We previously reported that high levels of M2-like CD204$^+$ TAMs correlated with tumour malignancy, had a detrimental effect on overall survival in patients with WHO Grades III–IV glioma, and possibly contributed to treatment resistance, while the TAM density in general showed little prognostic value [32]. Similar results have been published by others [35, 41]. Further, we found that CD204$^+$ TAMs co-expressed markers of both M1 and M2 activation as well as markers related to tumour aggressiveness. Further, CD204$^+$ TAMs tended to accumulate in areas surrounding blood vessels and necrosis suggesting a possible interaction with dedifferentiated stem-like glioma cells [32]. In this study, our aim was to explore the possible biological relevance of CD204 in glioblastoma. We examined by double immunohistochemistry the association between TAMs and glioblastoma cells expressing markers related to the stem-like phenotype. We also aimed to characterise CD204-enriched glioblastoma more thoroughly using the validated NanoString nCounter mRNA multiplex technology [42–44]. Lastly, we used immunohistochemistry and bioinformatics databases to confirm the gene expression profile of CD204-enriched glioblastoma and its prognostic value.

MATERIALS AND METHODS

Patient tissue

Archival formalin-fixed paraffin-embedded (FFPE) tissue samples from eight patients diagnosed with primary glioblastoma in 2006 were randomly included for the double immunohistochemical part of the study. For the NanoString gene expression part of the study, samples were obtained from the well-characterised Region of Southern Denmark glioma cohort [32, 45]. FFPE tissue specimens from 46 patients were included, and all patients had been diagnosed with primary glioblastoma between 2005 and 2009. The glioblastoma samples were selected based on their expression levels of CD204 and ionised calcium-binding adapter molecule-1 (IBA1), which had been determined by an immunofluorescence approach in our previous study [32], subdividing the 46 glioblastoma into four groups: (1) low levels of both CD204 and IBA1 (CD204^{LOW}/IBA1^{LOW}, $n = 12$); (2) high levels of both CD204 and IBA1 (CD204^{HIGH}/IBA1^{HIGH}, $n = 12$); (3) high and low levels of CD204 and IBA1, respectively (CD204^{HIGH}/IBA1^{LOW}, $n = 11$); and (4) low and high levels of CD204 and IBA1, respectively (CD204^{LOW}/IBA1^{HIGH}, $n = 11$). Isocitrate dehydrogenase (IDH) mutation and O6-methylguanine–DNA methyltransferase (MGMT) promoter status were assessed as previously described [32, 45]. An overview of patient characteristics including clinical and histological data is provided in Table 1. Based on their protein expression level of CD204 and IBA1, 20 of the 46 glioblastomas were included for immunohistochemical validation of some of the differentially deregulated genes found in the NanoString gene expression analysis.

All tissue samples were stained routinely with haematoxylin–eosin (H&E) to define representative tumour areas and reclassified by two pathologists according to WHO guidelines 2016 [1]. All patients underwent initial surgery at the Department of Neurosurgery, Odense University Hospital, Odense, Denmark.

Sample acquisition and RNA preparation

A total of 46 FFPE tissue samples were cut into 10-μm-thick sections on a microtome and mounted on glass slides. Guided by representative H&E stains, freshly cut sections were macrodissected to exclude areas with normal brain tissue and/or infiltrating tumour thereby

TABLE 1 Patient characteristics

		HR (95% CI)	p value
Patients (n)	46	—	—
Status (n)			
Alive/dead	0/46	—	—
Overall survival (months)			
Median (range)	8.70–30.7	—	—
Age			
Mean	65.6	1.03 (0.99–1.08)	0.10
Range	49.2–79.1	—	—
Sex (n)			
Male	22	1.00	0.38
Female	24	1.30 (0.72–2.34)	—
Performance status (n)			
0–1	22	1.00	—
2–4	24	1.44 (1.17–1.78)	<0.001
Tumour crossing midline (n)			
No	42	1.00	—
Yes	4	1.54 (0.54–4.44)[d]	0.42
Postsurgical treatment (n)			
Stupp[a]	24	1.00	—
Palliative treatment[b]	13	1.86 (0.91–3.81)	0.090
None[c]	9	117 (13.6–1011)[d]	<0.001
IDH status (n)			
Mutated	0	—	—
Wildtype	46	—	—
MGMT promoter status (n)			
Unmethylated	23	1.00	
Methylated	22	0.53 (0.28–1.03)	0.058
Not determined	1	—	—
CD204/IBA1 levels (n)			
Low/low	12	1.00	—
High/high	12	1.51 (0.65–3.48)	0.34
High/low	11	2.44 (1.02–5.86)	0.045
Low/high	11	1.06 (0.45–2.45)	0.90

[a]Treatment according to the publication by Stupp et al. [3].
[b]Palliative treatment is radiotherapy alone (60 Gy/30–33 fractions), hypofractionated radiotherapy alone (30–34 Gy/10 fractions), hypofractionated radiotherapy with chemotherapy, or chemotherapy alone.
[c]No postsurgical treatment.
[d]This hazard ratio should be interpreted with caution as n < 10.

enriching the amount of central tumour RNA in the subsequent gene expression analysis. Next, sections were detached from the glass slides and deparaffinised by subsequent submersion in a 3% glycerol solution and R-(+)-limonene followed by a washing step in absolute ethanol and rehydration in 3% glycerol. The tissue was then transferred to 1.5-ml Eppendorf tubes. Total RNA was extracted using the High Pure FFPET RNA Isolation Kit (Roche, Basel, Switzerland) according to the manufacturer's instructions. RNA quantity and quality was assessed using NanoDrop (Thermo Scientific, Waltham, MA, USA). Extracted RNA was stored at −80°C until further use.

NanoString gene expression analysis

mRNA gene expression analysis was performed using the NanoString barcode technology (NanoString Technologies, Seattle, WA, USA) with the NanoString nCounter® Human Myeloid Innate Immunity Panel v2 consisting of 770 genes and a customised CodeSet of 30 genes which was spiked into the standard myeloid panel. The customised 30-gene panel included the genes for CD204 (MSR1), the immune checkpoint marker galectin-9 (GAL9, LGALS9) [46], 26 genes related to cancer stemness [18, 19, 47, 48], glioma [1, 7], chemoresistance [15, 49] or the interferon pathway [50–52] as well as two additional housekeeping genes [53, 54] (File S1). Total RNA input was 150–250 ng with an A260/280 optical density between 1.61 and 1.99. Standard nCounter XT protocols were employed. Immediately after overnight hybridization, the target-probe complexes were purified and immobilised on the nCounter Prep Station followed by data collection and barcode counting in the nCounter Digital Analyser (nCounter® FLEX Analysis System, NanoString Technologies).

Conventional immunohistochemistry

Three μm sections from FFPE tissue blocks were mounted on FLEX IHC slides (Dako, Glostrup, Denmark). Immunohistochemical staining with unconjugated primary antibodies against baculoviral IAP repeat containing-3 (BIRC3), CD44, CD204, galectin-3 (GAL3), IBA1, intercellular adhesion molecule-1 (ICAM1) and tumour necrosis factor (TNF), alpha-induced protein-3 (TNFAIP3, also known as A20) were carried out on a fully-automated immunostainer (DISCOVERY ULTRA, Ventana Medical Systems, Inc., Tucson, AZ, USA). Standard protocols included deparaffinisation, epitope retrieval, and quenching of endogenous peroxidase followed by detection with the OptiView-HRP-DAB detection kit (Ventana). Immunostaining with primary antibodies against IL6, nucleotide-binding oligomerisation domain-containing protein 2 (NOD2) and programmed death-ligand 1 (PD-L1) were done semi-automatically using the Dako Autostainer Link 48 instrument and EnVision FLEX+ detection system (Agilent Technologies, Santa Clara, CA, USA). Tissue slides were counterstained using haematoxylin II and bluing reagent (Ventana protocols) or Mayer's haematoxylin (Autostainer protocols). Coverslips were mounted with Pertex® Mounting Medium (#00811, HistoLab Products AB, Gothenburg, Sweden). Information regarding primary antibodies, clone, epitope retrieval procedures, dilutions, incubation times and detection platforms is presented in Table S1.

Double immunohistochemistry

The protocols for the double immunohistochemical staining were designed as sequential application of unconjugated primary antibodies with heat deactivation steps in between each sequence for elution purposes. Adjacent sections of eight glioblastomas were stained with a panel of markers related to the stem-like phenotype (B lymphoma Mo-MLV insertion region 1 homologue [BMI1], CD44, CD133, musashi-1 [MSI1], nestin, podoplanin [PDPN] and [sex-determining region Y]-box 2 [SOX2]) [18, 19, 47] and the general microglial/macrophage marker IBA1 [55] or the M2-related marker CD204 [33]. Additionally, 20 glioblastomas were stained with antibodies against the immune checkpoint markers T-cell immunoglobulin and mucin-domain containing-3 (TIM3) and GAL9 [46]. See Data S1 and Table S2 for information regarding primary antibodies, clone, epitope retrieval procedures, dilutions, incubation times and detection platforms.

Quantitative digital image analysis

The stained slides were digitised using a NanoZoomer 2.0–HT whole slide scanner (Hamamatsu Photonics, Hamamatsu, Japan) equipped with a 40× objective. For the H&E, as well as the conventional single immunohistochemical staining, automated digital image analysis and quantification was performed using the Visiopharm Image Analysis Software, version 2018.4 (Hørsholm, Denmark) as previously reported [32, 56]. For each stain, the output variable was area fraction, which was defined as the positive area divided by the total tumour area. See Data S1 for additional information on the image analysis process. Estimates of necrosis were calculated in the Visiopharm software following manual delineation of areas containing vital tumour tissue and necrosis using digitised H&E stained slides. The necrotic component was defined as the area of necrosis divided by the area of total tumour tissue (i.e., necrosis + vital tumour tissue).

Quantification of the double immunostaining was done by stereological-based cell counting in the Visiopharm software. For the TIM3/GAL9 dual staining, sample images were acquired by systematic uniform random sampling at 20× magnification ensuring at least 10 images per tumour. Cell counting was performed using a 2×2 counting frame that covered 10% of the sampled image area. Reproducibility was tested by independently performing random sampling and cell counting twice on a training set of five glioblastoma specimens ($r_s = 1.00$, $p < 0.001$). Four different cell populations were counted: (1) negative cells (i.e., GAL9$^-$ TIM3$^-$), (2) GAL9$^+$ cells (i.e., GAL9$^+$ TIM3$^-$), (3) TIM3$^+$ cells (i.e., GAL9$^-$ TIM3$^+$) and (4) double$^+$ cells (i.e., GAL9$^+$ TIM3$^+$). Cell fractions were calculated based on the total cell count. For the stem-like cell marker and IBA1/CD204 double staining, cell counting was performed in three subregions for each tumour: (1) vital tumour area, (2) perivascular area and (3) perinecrotic area (Figure 1A1–A3). A maximum of five positions per subregion, when possible, were identified on a representative H&E for each tumour, and sample images were acquired for each double staining at 40x magnification. Cell counting was performed using a 1×1 counting frame that covered 30% of the sampled image area. CD204 and IBA1 served as internal controls for the counting system and tests of reproducibility ($r_s = 0.85$–0.96 for IBA1 and $r_s = 0.85$ for CD204, $p < 0.0001$). Following cell populations were counted: (1) tumour cells with stem-like cell phenotype (i.e., cells positive for the respective stem cell-related marker and negative for IBA1/CD204), (2) TAMs (i.e., IBA1$^+$ or CD204$^+$ cells) and (3) negative cells (i.e., cells negative for IBA1/CD204 and the respective stem cell-related marker). For the tumour cells expressing the stem cell-related marker, it was assessed whether they interacted directly with microglia/macrophage or not. Cells were categorised as proximal/interacting when they were directly adjacent with no other nuclei in between, and cells were classified as distal/non-interacting when one or more nuclei were located between the two cell populations. Similar evaluation was performed for CD204$^+$ cells with respect to CD133$^+$ and PDPN$^+$ tumour cells. Cell fractions were calculated based on the total cell count, the total number of tumour cells or the total number of CD204$^+$ cells.

Patient dataset analyses

mRNA expression data were explored using the GlioVis portal (http://gliovis.bioinfo.cnio.es/) [57]. Datasets were exported for the following genes: *IBA1* (*AIF1*), *CD204* (*MSR1*), *IL6*, *TNFAIP3*, *ICAM1*, *CD44*, *PD-L1* (*CD274*), *GAL3* (*LGALS3*), *GAL9* (*LGALS9*) and *TIM3* (*HAVCR2*), and used for survival analyses. Two different glioblastoma datasets were employed. From the Cancer Genome Atlas (TCGA), mRNA data were available for 324 patients diagnosed with primary IDH-wildtype glioblastoma (the Agilent 4502SA dataset) [58]. From the Gravendeel dataset [59], mRNA data were obtained for 91 patients with primary IDH-wildtype glioblastomas. Differential expression analysis was performed on both datasets to explore quantitative changes in gene expression levels between the groups of glioblastomas with the highest ($n = 120$ and $n = 37$, respectively) and lowest ($n = 123$ and $n = 40$, respectively) mRNA expression level of CD204. The lists of differential deregulated genes with log2 fold-change (FC) ≥ 1.5 or ≤ − 1.5 and adjusted $p < 0.05$ were exported directly from GlioVis for further analysis in the online resource STRING.

Statistics

Data files from the NanoString gene expression analyses were imported into the nSolver Analysis Software v4.0 with the Advanced Analysis Module 2.0 plugin (NanoString) for quality control, data normalisation and advanced analysis, including differential gene expression analyses, according to manufacturer's guidelines. p values were adjusted for multiple comparison by the Benjamini–Yekutieli false discovery rate (FDR) procedure [60].

The STRING online resource v11 (https://www.string-db.org/) [61] was accessed to conduct connectivity network analyses. Using the STRING resource Kyoto Encyclopedia of Genes and Genomes (KEGG) and Reactome enrichment analyses were performed for
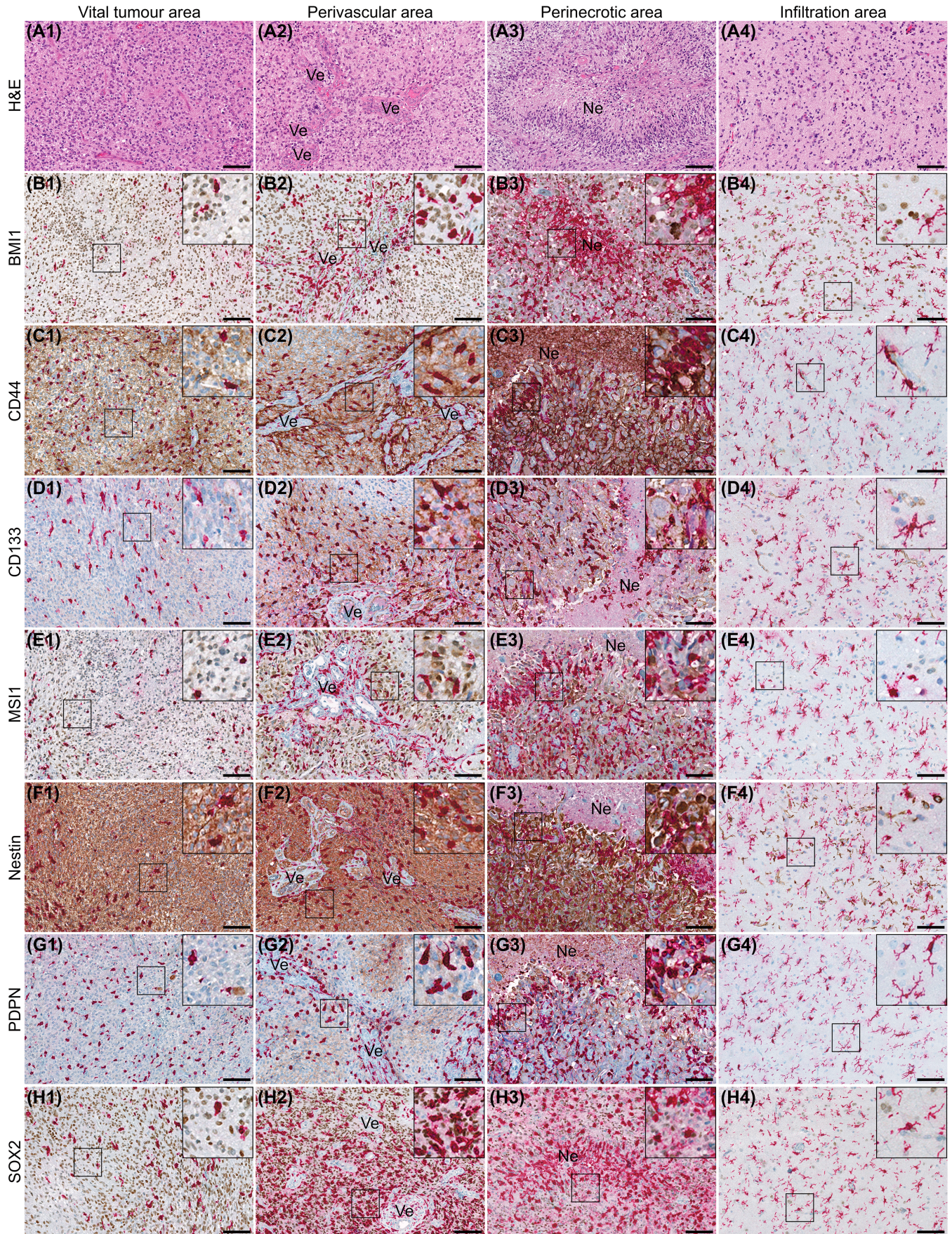
FIGURE 1 Legend on next page.

FIGURE 1 Expression of IBA1 and stem-like cell related markers in glioblastoma. Eight glioblastoma samples were stained using double immunohistochemistry with markers related to cancer stemness (*brown*) and IBA1 (*red*). IBA1$^+$ cells generally accumulated in perivascular and perinecrotic areas often showing an amoeboid morphology. IBA1$^+$ cells were morphologically ramified in the tumour infiltration area. (A1–A4) Representative haematoxylin–eosin (H&E) images of the different tumour subregions: Vital tumour area (A1), perivascular area (A2), perinecrotic area (A3), and tumour infiltration area (A4). (B1–B4) BMI1 expression appeared evenly distributed across the tumour and was also expressed in the infiltration area. (C1–C4) CD44 was widely expressed, but appeared more intense around necrotic areas and was rarely seen in the tumour infiltration area. (D1–D4) CD133 tumour cell density was higher in areas surrounding vasculature and necrosis. (E1–E4) MSI1$^+$ tumour cells were present in all tumour subregions showing a higher staining intensity in perivascular and necrotic areas, but was rarely observed in the tumour infiltration area. (F1–F4) Nestin was highly expressed in all tumour areas. (G1–G4) PDPN expression was primarily observed in perivascular and perinecrotic regions, while expression was limited in vital tumour and in the infiltration zone. (H1–H4) SOX2 was frequently expressed in all tumour subregions, but staining intensity seemed highest in vital and perivascular tumour areas. *Scale bar* 50 μM. *Abbreviations: BMI1*, B lymphoma Mo-MLV insertion region 1 homologue; *IBA1*, ionised calcium-binding adaptor molecule-1; *MSI1*, musashi-1; *Ne*, necrosis; *PDPN*, podoplanin; *SOX2*, sex-determining region Y-box 2; *Ve*, blood vessel

differentially regulated genes which had a log2 FC ≥ 1.50 and an FDR-adjusted $p < 0.05$. STRING network analyses were set to require a minimum interaction score of 0.70 or 0.40 (high and medium confidence, respectively), and network clustering was performed by applying the Markov cluster (MCL) algorithm with a inflation parameter of 1.8 [62].

An expression-based heatmap was generated using the web server Heatmapper (available at http://www.heatmapper.ca/) [63] to visualise and cluster the results of the quantitative staining analyses. Unsupervised hierarchical clustering was conducted based on the Euclidean distance and complete linkage methods.

Student's unpaired *t* test or its non-parametric equivalent Mann–Whitney *U*-test was used when comparing two groups. One-way ANOVA with Bonferroni's multiple comparison test or the non-parametric Kruskal–Wallis test with Dunn's multiple comparison test was used to compare more than two groups. Correlation analyses were conducted by Spearman's rank-order correlation coefficient. Survival functions were illustrated using the Kaplan–Meier estimator. Overall survival was defined as time from primary surgery until death or date of censoring. Survival distributions were compared using the log-rank test. Multivariate analyses were conducted using the Cox proportional-hazards model to obtain hazard ratios (HRs). All Cox models were tested for proportional hazard, time-dependency and interaction effects of the explanatory factors. The median value of the investigated biomarkers was used as pre-specified cut-off value. The statistical analyses were carried out in STATA v16 (StataCorp LLC, College Station, TX, USA) or Prism 5.0 (GraphPad Software Inc., San Diego, CA, USA). $p < 0.05$ were considered statistically significant.

RESULTS

Tumour-associated microglia/macrophages accumulate in perivascular and perinecrotic areas often in close proximity to dedifferentiated/stem-like glioblastoma cells

IBA1$^+$ TAMs were present in all samples often in moderate numbers and often displayed an amoeboid morphology. Significantly higher densities were observed in perivascular and perinecrotic areas,

including areas of pseudo-palisading necrosis, compared with the vital tumour area ($p < 0.05$), comprising approximately 40% of the total cell count in these areas (Figures 1 and 2A). Morphologically more ramified IBA1$^+$ cells were observed in the tumour infiltration area.

BMI1 was expressed in all tumours and appeared evenly distributed throughout the whole tumour; however, the staining intensity seemed to decrease in perinecrotic areas (Figure 1B1–B4). No significant difference in BMI1$^+$ cell density was observed among in different tumour subregions ($p = 0.44$) (Figure 2A), and the interaction rate between BMI1$^+$ and IBA1$^+$ cells did not show any significant subregional differences ($p = 0.21$) (Figure 2B).

CD44 was widely expressed (Figure 1C1–C3) regardless of tumour area ($p = 0.31$) (Figure 2A), and no subregional difference in microglial interaction was observed ($p = 0.71$) (Figure 2B). The staining intensity appeared higher in perinecrotic areas, while CD44 lacked or was only weakly expressed by a few cells in the infiltration zone (Figure 1C4).

CD133 was mostly expressed in areas surrounding vascular structures and necroses displaying more intense staining in these areas compared to vital tumour areas and the tumour infiltration zone (Figure 1D1–D4). The CD133$^+$ tumour cell density (Figure 2A) was higher in the perivascular ($p < 0.001$) and perinecrotic areas ($p < 0.01$) relative to the vital tumour area, but the ratio of CD133$^+$ cells interacting with IBA1$^+$ cells did not differ among the three subregions ($p = 0.54$) (Figure 2B).

MSI1 showed high inter-tumoural heterogeneity. The staining intensity seemed to increase in perivascular and perinecrotic areas compared to vital tumour tissue and the infiltration area (Figure 1E1–E4); however, no significant differences were found among the tumour subregions ($p = 0.27$) (Figure 2A). In tumours with high MSI1 levels in general, MSI1 was expressed in all areas regardless of the number of IBA1$^+$ cells. In tumours with lower expression levels, MSI1$^+$ cells tended to accumulate in IBA1-rich areas especially in the perivascular regions (data not shown); however, overall, no significant difference in the interaction rate was found ($p = 0.36$) (Figure 2B).

Nestin was widely expressed in most tumours independent of the tumour subregion ($p = 0.78$) (Figures 1F1–F4 and 2A). In the perivascular areas, the ratio of nestin$^+$ tumour cells interacting with IBA1$^+$ cells was significantly higher in the perivascular area compared to the vital tumour area ($p < 0.05$ (Figure 2B).
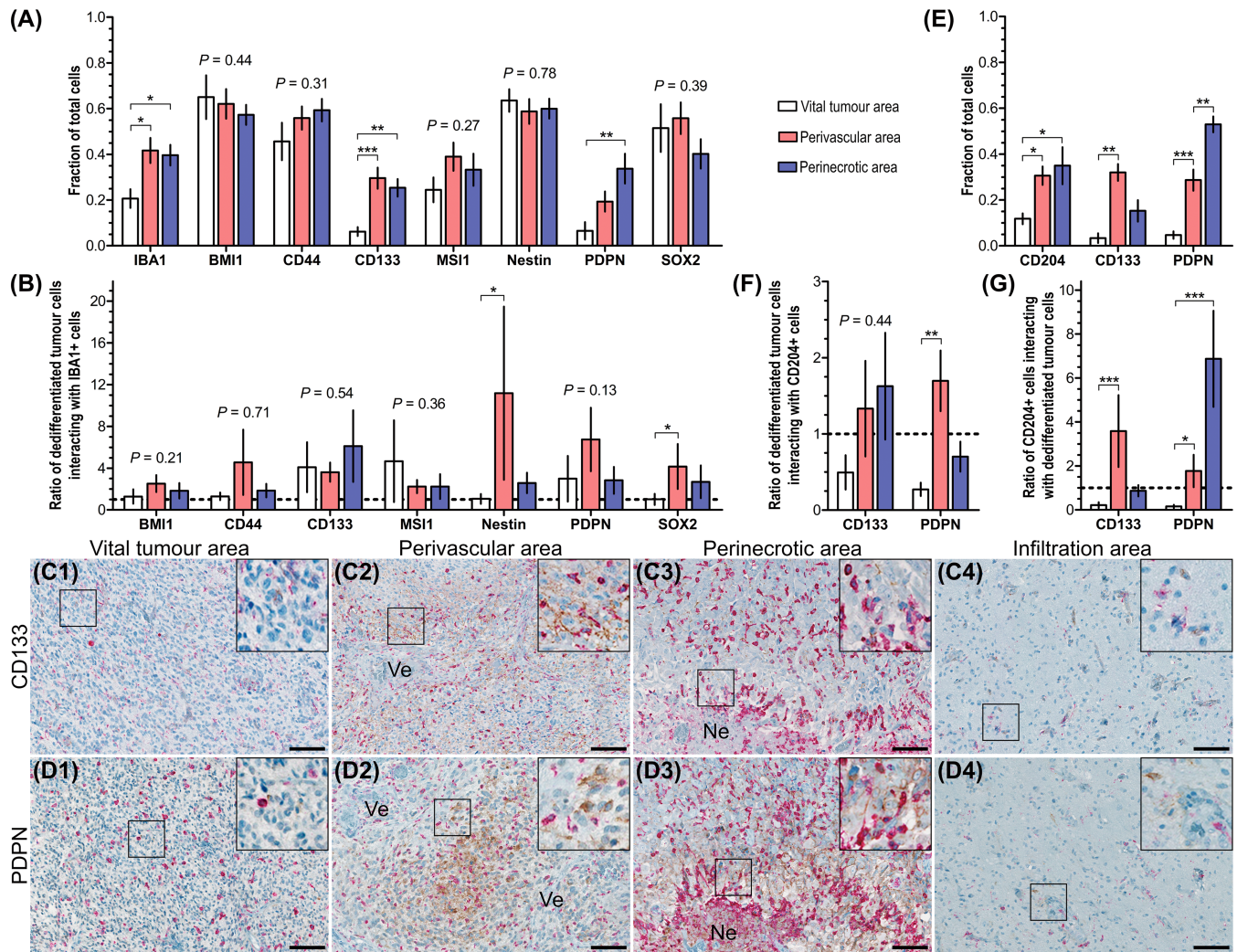
FIGURE 2 Quantitative estimates of the expression and interaction levels of IBA1, CD204 and stem-like cell related markers in glioblastoma. (A) Quantification of the IBA1 double immunohistochemistry stains showed that the fractions of IBA1$^+$ TAMs as well as CD133$^+$ tumour cells were significantly higher in perivascular and perinecrotic areas relative to vital tumour. The fraction of PDPN$^+$ tumour cells was significantly higher in areas of necrosis compared with vital tumour regions and tended to be higher in perivascular regions. (B) BMI1$^+$, CD44$^+$, CD133$^+$ and MSI1$^+$ tumour cells did not interact significantly with IBA1$^+$ TAMs in any of the tumour subregions. Nestin$^+$ and SOX2$^+$ tumour cells often interacted with IBA1$^+$ TAMs in areas surrounding vasculature, and similar tendency was found for PDPN$^+$ tumour cells. (C,D) CD204, CD133 and PDPN expression levels were elevated in perivascular and perinecrotic areas compared with vital tumour area and were rarely observed in the infiltration zone. (E) Quantification of the CD204 double immunohistochemistry stains showed that the fractions CD204$^+$ TAMs and PDPN$^+$ tumour cells were significantly higher in perivascular and perinecrotic areas relative to vital tumour area, while the fraction of CD133$^+$ tumour cells was especially high in the perivascular region. (F) Looking at the CD133$^+$ tumour population, the ratio of CD133$^+$ tumour cells interacting with CD204$^+$ TAMs did not differ among the three subregions. Looking at the PDPN$^+$ tumour population, the ratio of PDPN$^+$ tumour cells were in direct contact with CD204$^+$ TAMs was significantly higher in the perivascular area relative to the vital tumour area. (G) CD204$^+$ TAMs were rarely in contact with CD133$^+$ and PDPN$^+$ tumours cell in the vital tumour, but significantly interacted with CD133$^+$ and PDPN$^+$ tumour cells in the perivascular area and exhibited an especially high interaction rate with PDPN$^+$ tumour cells in the perinecrotic area. Horizontal and vertical lines indicate mean ± SEM. *$p < 0.05$; **$p < 0.01$; ***$p < 0.001$. *Scale bar* 50 μM. *Abbreviations: BMI1*, B lymphoma Mo-MLV insertion region 1 homologue; *IBA1*, ionised calcium-binding adaptor molecule-1; *MSI1*, musashi-1; *Ne*, necrosis; *PDPN*, podoplanin; *SOX2*, sex-determining region Y-box 2; *Ve*, blood vessel

PDPN$^+$ tumour cells were only sporadically observed in vital tumour areas and absent in the tumour-infiltrating area. Instead, PDPN$^+$ cells particularly accumulated in perinecrotic areas ($p < 0.01$) (Figure 1G1–G4 and Figure 2A) and tended to directly interact with IBA1$^+$ cells in the perivascular region ($p = 0.13$) (Figure 2B).

SOX2 was expressed in all tumours. The staining intensity appeared higher in vital tumour tissue and around blood vessels compared to perinecrotic areas and the infiltration zone (Figure 1H1–H4), but the fraction of SOX2$^+$ cells was similar across the different tumour subregions ($p = 0.39$) (Figure 2A). However, in the

perivascular area, the SOX2$^+$ cells significantly co-localised with IBA1$^+$ cells compared to the vital tumour area ($p < 0.05$) (Figure 2B).

As the presence of especially CD133$^+$ and PDPN$^+$ tumour cells was higher in the perivascular and perinecrotic niches, we chose to investigate the level of co-location with CD204$^+$ TAMs for these two markers only. We found similar regional expression patterns when investigating the CD204/CD133 (Figure 2C1–C4) and CD204/PDPN double staining (Figure 2D1–D4) with increased expression levels around blood vessels and areas of necrosis (Figure 2E). In the perinecrotic areas, the fraction of CD204$^+$ cells was almost the same to that of IBA1 constituting approximately 40% of cells, while the CD204$^+$ cells were less frequent in the perivascular and vital tumour areas relative to the IBA1$^+$ cells (Figure 2A,E). Looking at the tumour cell populations, limited interaction was observed between CD133$^+$ tumour cells and CD204$^+$ cells (Figure 2F), while the fraction of PDPN$^+$ tumour cells in direct contact with CD204$^+$ cells was significantly higher in the perivascular area relative to vital tumour area ($p < 0.01$) (Figure 2F). Looking specifically at the CD204$^+$ TAMs, the ratio of CD204$^+$ cells interacting directly with CD133$^+$ cells was higher in the perivascular area than in the vital tumour area ($P < 0.001$), and a similar increase in interaction rate was found for CD204$^+$ and PDPN$^+$ cells in both the perivascular ($P < 0.05$) and perinecrotic area ($P < 0.001$) compared with the vital tumour area (Figure 2G).

Overall, IBA1$^+$ and CD204$^+$ cells (i.e., TAMs) seemed to accumulate in perivascular and perinecrotic areas showing close interaction with tumour cells expressing PDPN in perivascular and perinecrotic regions.

CD204-enriched glioblastomas display a unique gene expression profile and associate with necrosis

Myeloid mRNA profiling was performed on 46 glioblastomas using the NanoString barcode technology. The 46 glioblastomas were selected and subdivided into four groups based on their protein levels of CD204 and IBA1. A scatter plot illustrating the four groups and their expression levels is shown in Figure 3A. The level of IBA1 and CD204 protein co-expression was significantly highest in the CD204^{HIGH}/IBA1^{LOW} group (Figure 3B). Patients in the CD204^{HIGH}/IBA1^{LOW} group had the poorest survival outcome in both the univariate (HR 2.44, $p = 0.045$) (Figure 3C and Table 1) and multivariate analysis (HR 3.54, $p = 0.015$) (Figure 3D). A heatmap of the normalised mRNA data generated via unsupervised hierarchal clustering revealed that two major clusters existed within the glioblastomas (Figure 3E). Cluster 1 primarily comprised tumours of the CD204^{LOW}/IBA1^{LOW} and CD204^{LOW}/IBA1^{HIGH} groups, whereas Cluster 2 mainly consisted of tumours with high CD204 levels (i.e., the CD204^{HIGH}/IBA1^{HIGH} and CD204^{HIGH}/IBA1^{LOW} groups). Survival analysis showed that Cluster 2 was associated with poorer prognosis (HR 2.01, $p = 0.026$) (Figure 3F), also independent of performance status, postsurgical treatment, and MGMT status (HR 3.19, $p = 0.004$) (Figure 3G), but the cluster pattern was

not a stronger prognosticator of survival than the CD204/IBA1 signature.

Pathway scoring was used to condense the gene expression profile of each sample into a set of 47 pathway scores. Unsupervised cluster analyses re-identified the two clusters described above, and a high level of pathway activity was observed in Cluster 2 compared with Cluster 1, predominantly due to low pathway scores in the CD204^{LOW}/IBA1^{LOW} samples (Figures 4A and S1). Many of the pathways were related to the immune response. To better characterise the immune composition of the glioblastoma samples, raw cell type abundances were measured for macrophages, cytotoxic cells and neutrophils. As expected the CD204^{LOW}/IBA1^{LOW} group displayed the lowest measurements for all three immune cell populations, especially macrophages and neutrophils ($p < 0.001$) (Figure 4B). Because immune activation may be initiated by necrosis and depend on cellular density within the tumour, the presence of necrosis and cellularity/cell density were estimated in all 46 samples (Figure S2). These analyses showed that necrotic areas were more frequently observed in glioblastomas with high protein expression of primarily CD204 ($p < 0.01$) (Figure 4C). Inversely, CD204-enriched glioblastomas had significantly lower cellularity ($p < 0.05$) (Figure 4D).

CD204-enriched glioblastomas are immunologically inflamed tumours and have a mixed M1/M2 phenotype

Genes included in the NanoString panel were tested for differential expression in response to the CD204/IBA1 subgroups using the CD204^{LOW}/IBA1^{LOW} group as baseline. Gene set analyses (GSA) were performed by summarising the results of the differential expression analysis at gene set level identifying the most differentially expressed genes. The extent of differential expression in each gene set was then measured using a global significance score. GSA showed that expression levels of genes involved in complement coagulation cascades, NOD-like receptor and TNF signalling pathways, transport and catabolism, immune diseases, and infectious diseases were higher in CD204-rich tumours (Figure S3). Mapping the differentially expressed genes to KEGG pathways supported the observation that the differentially expressed genes were enriched for the TNF signalling pathway, but also for additional signalling pathways, for example, Toll-like receptor (TLR), chemokine, nuclear factor kappa B (NF-kappa B), and Janus kinases-signal transducer and activator of transcription protein (Jak-STAT) as well as in pathways related to phagosome, cytokine-cytokine receptor interaction, cell adhesion molecules (CAMs), proteoglycans and transcriptional misregulation in cancer (Table S3). Focusing on the differentially deregulated genes, 164 and 87 genes were significantly (adj. $p < 0.05$) ≥1.50-fold upregulated in the CD204^{HIGH}/IBA1^{HIGH} and CD204^{HIGH}/IBA1^{LOW} groups, respectively, relative to the CD204^{LOW}/IBA1^{LOW} baseline group. Among the highest upregulated genes were *CCL20, IL6, CXLC14, CXCL8* [IL8], *ICAM1, OSM, S100A8, S100A9* and *PD-L1* (Figure 4E,F and Table 2). The CD204-enriched groups expressed genes related to both the M1
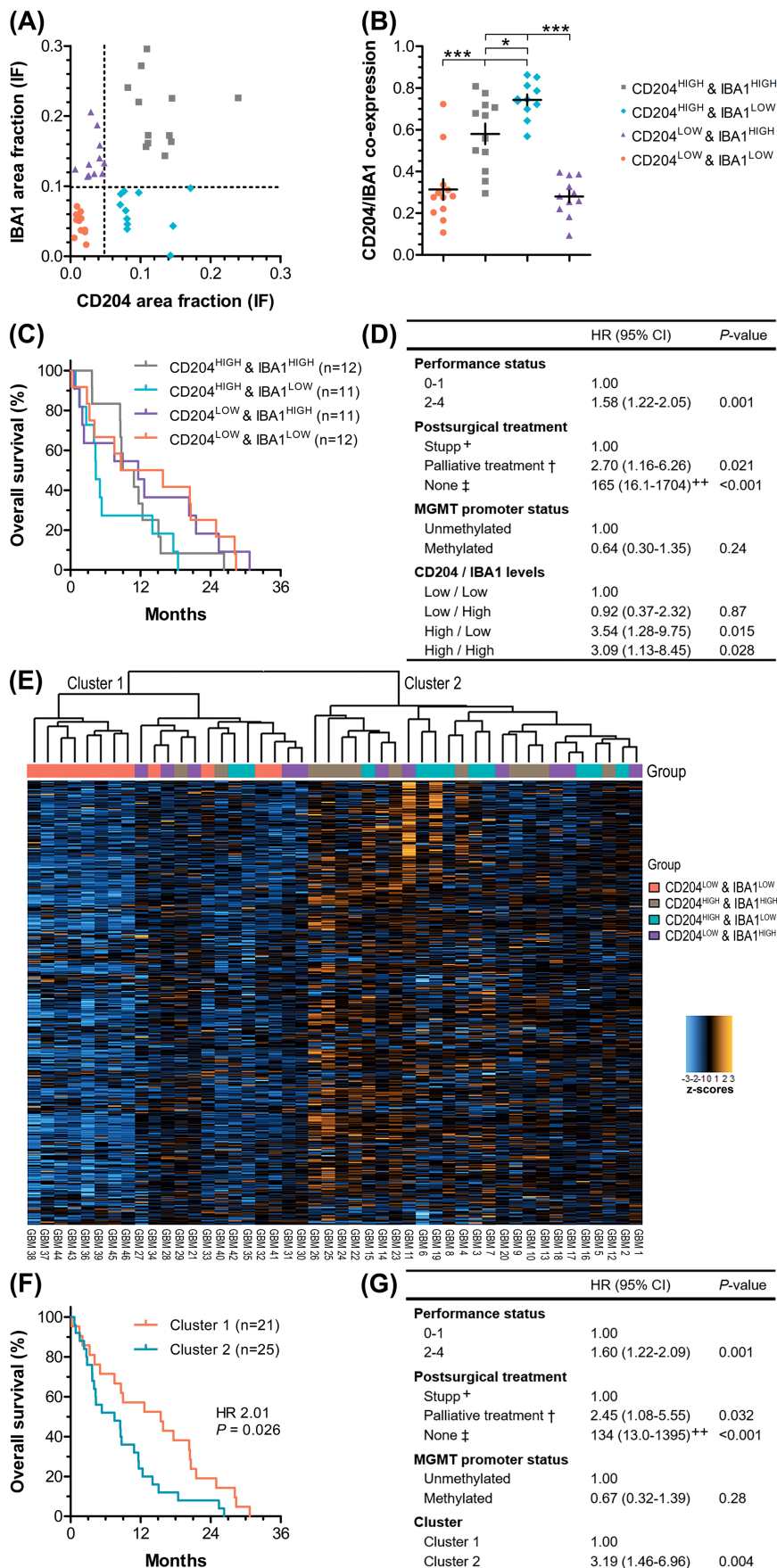
FIGURE 3 Legend on next page.

FIGURE 3 The prognostic value of the CD204/IBA1 signature and gene expression profiling of CD204-enriched glioblastomas. (A) A total of 46 glioblastomas were included for gene expression profiling using the NanoString barcode multiplex technology. The 46 samples were selected based on the CD204 and IBA1 expression levels, which had been determined previously using double immunofluorescence. This resulted in a subdivision of the samples into four groups: CD204^{LOW}/IBA1^{LOW} ($n = 12$), CD204^{HIGH}/IBA1^{HIGH} ($n = 12$), CD204^{HIGH}/IBA1^{LOW} ($n = 11$), and CD204^{LOW}/IBA1^{HIGH} ($n = 11$). (C) The CD204^{HIGH}/IBA1^{LOW} group also exhibited the highest level of CD204-IBA1 co-expression. (C,D) Kaplan–Meier plot illustrating that the patients in the CD204^{HIGH}/IBA1^{LOW} and CD204^{HIGH}/IBA1^{HIGH} groups had the worst survival in both the univariate and multivariate analyses. (E) Heatmap generation and unsupervised hierarchical clustering of the normalised data from the NanoString analysis identified two major clusters. Cluster 1 mostly comprised glioblastomas of the CD204^{LOW}/IBA1^{LOW} group, whereas Cluster 2 consisted of tumours with high CD204 levels. (F,G) Log-rank and cox regression analyses showed that Cluster 2 correlated with shorter overall survival. $^{+}$ Treatment according to the publication by Stupp et al. [3]. †Palliative treatment is radiotherapy alone (60 Gy/30–33 fractions), hypofractionated radiotherapy alone (30–34 Gy/10 fractions), hypofractionated radiotherapy with chemotherapy or chemotherapy alone. ‡No postsurgical treatment. $^{++}$This hazard ratio should be interpreted with caution as $n < 10$
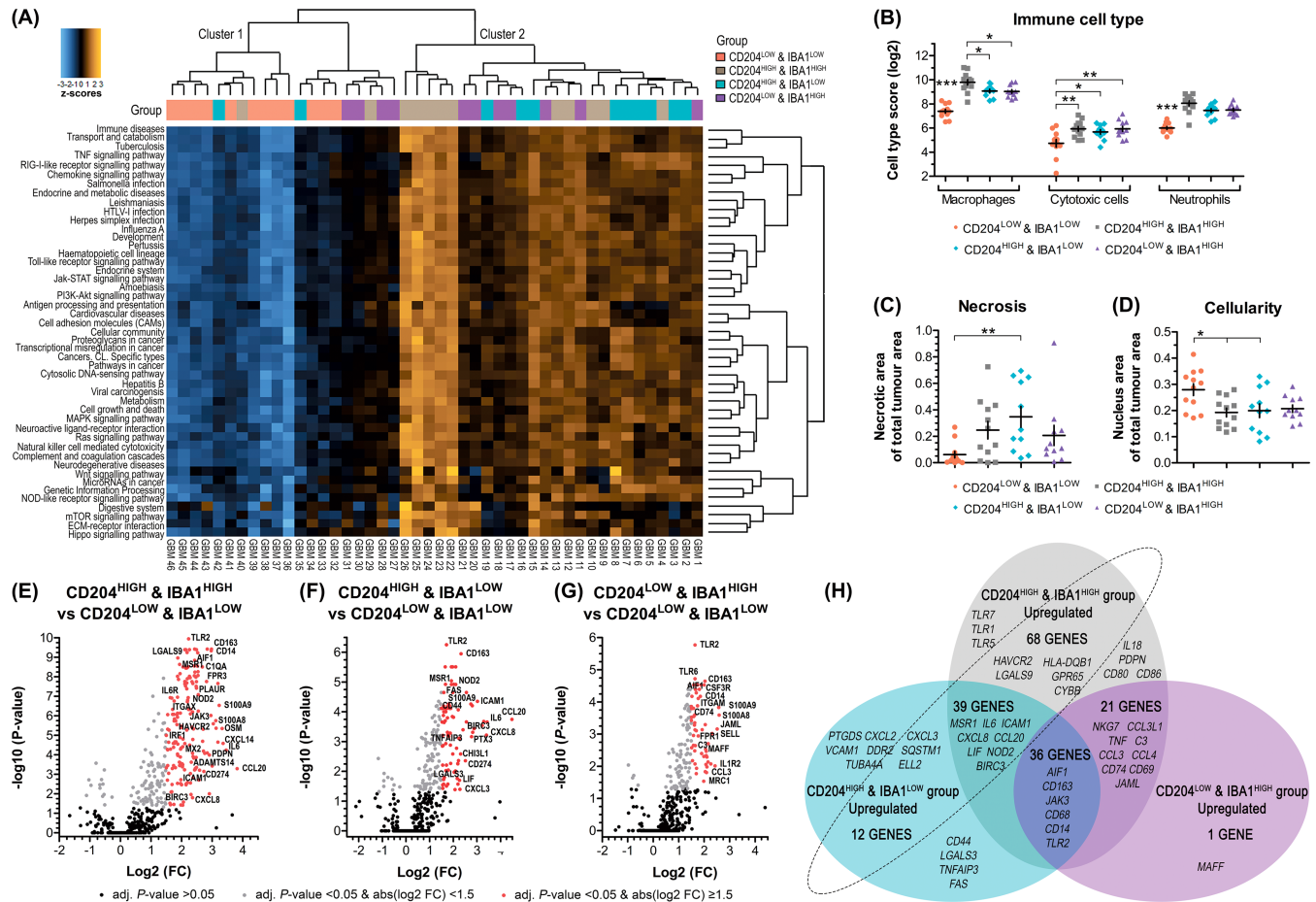
FIGURE 4 Altered gene expression pattern in CD204-enriched glioblastomas. (A) Condensing the gene expression profile of each sample provided a set of pathway scores and generated a heatmap. Unsupervised cluster analysis generated a cluster pattern similar to the one seen for the normalised gene expression data. Cluster 2 mainly comprised CD204-enriched glioblastomas and was associated with a higher level of pathway activity. (B) Cell type abundance measurements showed that glioblastomas with low levels of TAMs (i.e., the CD204^{LOW}/IBA1^{LOW} group) displayed in lowest levels of macrophages (based on the mRNA levels of *CD163, CD68* and *CD84*), cytotoxic cells (based on the mRNA levels of *NKG7* and *KLRK1*), and neutrophils (based on the mRNA levels of *FPR1, SIGLEC5, CSF3R* and *FCGR3A*). (C) Assessment of the necrotic component revealed that necrosis was more common in glioblastomas with high CD204 expression. (D) Estimation of cellularity showed that glioblastomas with high CD204 levels had lower cell density. (E) Differential gene expression analysis revealed that 164 of 585 genes were significantly upregulated above 1.50 log2 fold-change (FC) in the CD204^{HIGH}/IBA1^{HIGH} group relative to the CD204^{LOW}/IBA1^{LOW} group. (F) Differential gene expression analysis revealed that 87 of 585 genes were significantly upregulated above 1.50 log2 FC in the CD204^{HIGH}/IBA1^{LOW} group relative to the CD204^{LOW}/IBA1^{LOW} group. (G) Differential gene expression analysis revealed that 58 of 585 genes were significantly upregulated above 1.50 log2 FC in the CD204^{LOW}/IBA1^{HIGH} group relative to the CD204^{LOW}/IBA1^{LOW} group. (H) Graphical representation of the overlap of the differentially upregulated genes in the CD204^{HIGH}/IBA1^{HIGH}, CD204^{HIGH}/IBA1^{LOW} and CD204^{LOW}/IBA1^{HIGH} groups relative to the CD204^{LOW}/IBA1^{LOW} group showed that 119 genes were uniquely upregulated in CD204^{HIGH} (i.e., CD204-enriched) glioblastomas. Horizontal and vertical lines indicate mean $\pm$ SEM. $^{*}p < 0.05$; $^{**}p < 0.01$; $^{***}p < 0.001$

TABLE 2 List of differentially expressed genes ($n = 119$) in CD204^{HIGH} tumours

	CD204^{HIGH} & IBA1^{HIGH} vs. CD204^{LOW} & IBA1^{LOW}		CD204^{HIGH} & IBA1^{LOW} vs. CD204^{LOW} & IBA1^{LOW}	
	Log2 FC	Adj. p value	Log2 FC	Adj. p value
Genes only differentially upregulated in CD204^{HIGH} tumours ($n = 39$)				
ADAM8	2.84	8.10E-05	2.09	9.72E-03
ADAMTS14	2.32	2.39E-04	1.56	3.72E-02
ALDH1A1	1.87	2.93E-03	1.89	5.44E-03
ALOX5AP	2.34	1.79E-08	1.92	1.21E-05
BIRC3	1.75	3.56E-02	2.88	3.70E-04
C5AR1	2.22	1.17E-07	1.81	5.48E-05
CCL2	2.49	4.41E-04	2.22	4.38E-03
CCL20	3.82	5.18E-04	4.48	1.80E-04
CD274	2.73	7.15E-04	2.51	4.41E-03
CHI3L1	2.45	5.11E-04	2.31	2.62E-03
CSF1	1.77	1.46E-06	1.59	6.41E-05
CTSD	1.68	1.23E-07	1.66	3.09E-06
CXCL1	2.06	2.65E-02	2.07	4.11E-02
CXCL14	3.36	2.62E-05	2.17	1.74E-02
CXCL8	2.36	1.60E-02	3.40	6.06E-04
DPP4	2.43	6.02E-04	2.04	1.06E-02
FOSL1	2.04	3.26E-04	1.71	6.20E-03
ICAM1	1.97	3.00E-03	3.02	4.47E-05
IL1R1	2.38	1.25E-04	2.24	7.87E-04
IL4I1	2.17	5.38E-06	1.96	1.44E-04
IL6	3.46	5.75E-05	3.43	2.20E-04
LIF	3.00	3.74E-04	2.26	2.01E-02
MAFB	2.23	4.71E-07	1.75	1.59E-04
MAPK13	2.48	3.09E-08	2.10	1.21E-05
MMP19	2.15	3.15E-03	2.19	5.59E-03
MSR1	2.17	3.49E-09	1.67	1.20E-05
MX2	2.27	3.17E-05	1.88	1.31E-03
NAMPT	1.74	3.58E-04	2.01	1.52E-04
NCF2	2.17	4.15E-08	1.92	9.07E-06
NFKBIZ	1.87	9.23E-05	1.77	6.12E-04
NOD2	2.20	1.58E-07	2.02	1.20E-05
OSCAR	1.96	7.28E-07	1.66	7.70E-05
PLAUR	2.49	3.81E-08	1.84	7.70E-05
PTGS2	1.98	3.77E-02	2.20	2.69E-02
PTX3	2.59	6.24E-04	2.77	6.87E-04
SERPINE1	2.10	5.90E-04	1.59	2.69E-02
SIGLEC1	2.72	6.51E-05	1.77	2.69E-02
TGM2	1.96	1.30E-04	1.55	6.20E-03
TNFRSF14	1.54	5.31E-05	1.58	1.33E-04
Genes only differentially upregulated in CD204^{HIGH} & IBA1^{LOW} tumours ($n = 12$)				
CD44	—	—	1.73	7.70E-05
CXCL2	—	—	1.69	9.45E-03

(Continues)

TABLE 2 (Continued)

	CD204^{HIGH} & IBA1^{HIGH} vs. CD204^{LOW} & IBA1^{LOW}		CD204^{HIGH} & IBA1^{LOW} vs. CD204^{LOW} & IBA1^{LOW}	
	Log2 FC	Adj. p value	Log2 FC	Adj. p value
CXCL3	—	—	2.28	4.00E-02
DDR2	—	—	1.84	6.41E-05
ELL2	—	—	1.50	7.70E-05
FAS	—	—	1.60	2.24E-05
LGALS3	—	—	1.59	1.87E-02
PTGDS	—	—	3.29	2.11E-04
SQSTM1	—	—	1.80	6.41E-05
TNFAIP3	—	—	1.68	1.17E-03
TUBA4A	—	—	1.79	9.07E-03
VCAM1	—	—	1.98	2.62E-03
Genes only differentially upregulated in CD204^{HIGH} & IBA1^{HIGH} tumours ($n = 68$)				
ADORA3	2.05	1.55E-05	—	—
AOAH	1.93	2.39E-04	—	—
BTK	2.14	3.55E-09	—	—
CASP1	1.78	2.17E-05	—	—
CCRL2	1.71	8.46E-07	—	—
CD180	2.04	3.89E-05	—	—
CD80	2.03	4.14E-04	—	—
CD84	2.18	5.68E-10	—	—
CD86	1.98	4.09E-06	—	—
CEBPA	1.82	2.18E-05	—	—
CEBPB	1.50	1.02E-05	—	—
CLEC5A	1.88	2.83E-05	—	—
CSF1R	2.13	2.99E-08	—	—
CSF2RA	1.59	5.38E-06	—	—
CTSL	1.50	4.69E-04	—	—
CTSS	2.17	2.06E-08	—	—
CX3CR1	1.66	8.16E-03	—	—
CXCL12	2.19	2.69E-03	—	—
CYBB	2.42	2.76E-09	—	—
EGR2	1.69	3.34E-03	—	—
ENPP2	1.64	3.68E-02	—	—
GATA3	1.62	3.11E-02	—	—
GPR65	2.55	8.30E-08	—	—
HAVCR2	1.85	2.81E-06	—	—
HBEGF	1.70	5.11E-04	—	—
HLA-DMA	1.76	1.85E-06	—	—
HLA-DMB	1.87	1.12E-07	—	—
HLA-DPB1	1.64	5.19E-05	—	—
HLA-DQB1	2.91	1.01E-02	—	—
HLA-DRA	1.55	5.61E-05	—	—
HPGDS	2.02	2.92E-04	—	—
IER3	1.73	2.60E-05	—	—

TABLE 2 (Continued)

	CD204^{HIGH} & IBA1^{HIGH} vs. CD204^{LOW} & IBA1^{LOW}		CD204^{HIGH} & IBA1^{LOW} vs. CD204^{LOW} & IBA1^{LOW}	
	Log2 FC	Adj. *p* value	Log2 FC	Adj. *p* value
IGF1	2.04	3.83E-02	—	—
IL15RA	1.75	8.46E-07	—	—
IL17RA	1.55	8.80E-07	—	—
IL18	2.19	1.91E-07	—	—
IL4R	1.85	8.80E-07	—	—
IL6R	1.63	1.17E-07	—	—
IRF1	1.58	2.28E-05	—	—
IRF5	1.71	4.70E-07	—	—
IRF8	1.77	2.56E-05	—	—
ITGAL	1.96	2.64E-04	—	—
ITGAX	1.76	1.74E-07	—	—
LAT2	1.90	1.36E-08	—	—
LGALS9	1.88	1.07E-09	—	—
LST1	1.58	8.86E-04	—	—
MPEG1	1.94	3.58E-04	—	—
NLRP3	1.55	3.56E-04	—	—
PDPN	2.91	1.04E-04	—	—
PIK3CG	2.11	1.76E-08	—	—
PLAU	1.68	8.01E-03	—	—
PTAFR	1.94	2.30E-09	—	—
PYCARD	2.21	3.11E-09	—	—
RUNX2	2.31	1.08E-02	—	—
S100A4	1.99	4.49E-05	—	—
SIGLEC5	1.88	1.09E-04	—	—
STAT6	1.55	4.91E-06	—	—
SYK	2.26	4.08E-10	—	—
TLR1	1.95	6.96E-09	—	—
TLR5	1.80	4.63E-04	—	—
TLR7	2.45	5.53E-04	—	—
TNFAIP8	1.81	1.85E-06	—	—
TNFRSF11A	1.87	7.35E-07	—	—
TNFRSF1B	1.87	9.51E-09	—	—
TNFSF10	2.11	2.65E-05	—	—
TREM2	2.14	4.08E-10	—	—
TYROBP	2.11	2.30E-08	—	—
WAS	2.11	4.08E-10	—	—

(e.g., *CD80, CD86, IL18, IL1R1, CCL2, IL15, IL1B, CCL5* and *HLA*) and M2 (*TLR1, TGM2,* CD204 [*MSR1*], CD206 [*MRC1*], *IL1R2* and *CD163*) polarisation profiles [10, 33, 38, 64–66]. In the CD204^{LOW}/IBA1^{HIGH} group, 58 genes, including *S100A8, S100A9, JAML* [AMICA1] and *OSM*, were ≥1.50-fold upregulated compared with baseline (Figure 4G and Table S4). The IBA1-enriched group differentially expressed, in particular, M1-related genes (*TLR2, TNF, CCL3, CCL4, IL15, IL1B* and *CCL5*), but also some M2-related genes (*CD206, IL1R2* and *CD163*). No genes were differentially downregulated below a log2 FC of −1.50 in any of the three subgroups relative to the CD204^{LOW}/IBA1^{LOW} group. Among the genes related to cancer stemness, only *ALDH1A1* [aldehyde dehydrogenase 1 family, member A1], *CD44* and *PDPN* had significant log2 FC ≥ 1.50 and only in CD204^{HIGH} tumours (Table S5). None of the glioblastoma-related genes were differentially

expressed (Table S5). File S2 lists all genes identified with differential expression analysis in the corresponding groups.

IL6 plays a central role in the genetic interaction network in CD204-enriched glioblastomas

To identify genes that were exclusively upregulated in CD204^{HIGH} glioblastomas, the differentially upregulated genes from all three subgroups were investigated for potential overlap (Figure 4H), and 119 genes were found to be upregulated only in CD204^{HIGH} glioblastomas including *CD204*, *IL6*, *ICAM1*, *PD-L1*, *BIRC3* and *CCL20* (Table 2), while 22 upregulated genes were shared only between the IBA1^{HIGH} groups including *C3*, *C1QA*, *C1QB*, *CCL3*, *CD74* and *TNF* (Table S6), and 36 genes were shared among all three subgroups compared with the baseline group including *IBA1*, *S100A8* and *S100A9* (Table S7). The 119 genes that were uniquely upregulated in the CD204^{HIGH} glioblastoma showed a strong interaction enrichment when performing STRING connectivity analysis, and cluster analysis identified three major and three minor clusters that were interconnected (Figure 5A). The biggest cluster (*red*) appeared to centre on *IL6*, which was the gene with the highest number of gene–gene interactions (Figure 5B). *IL6* connected either directly or indirectly, for example, via *CCL2*, *ICAM1*, *CXCL8* and *IRF1* with the other subnetworks including the second biggest cluster (*yellow*) which comprised *HLA* genes, *IRF1*, *CD44* and *PD-L1* among others. Both *CD44* and *PD-L1* were connected to a smaller cluster (*blue*) consisting of the immune checkpoint markers *TIM3* and *GAL9* as well as *GAL3*. KEGG and Reactome Pathway analyses demonstrated an overrepresentation of terms related to activation and regulation of the immune system as well as cellular communication by cytokines or chemokines including 'Cytokine–cytokine receptor interaction', 'TNF signalling pathway', 'NOD-like receptor signalling pathway', 'NF-kappa B signalling pathway' and 'Interferon signalling'. The upregulated genes were also involved in 'Extracellular matrix organisation', 'haemostasis', 'transcriptional misregulation in cancer' as well as various autoimmune and infectious diseases. Further, the signalling pathways related to promotion of the M2 polarisation phenotype (i.e., IL10, IL4 and IL13 [10, 33, 64–66]) were overrepresented (Figure 5C,D and Tables S8,S9). Connectivity and enrichment analyses of the 36 shared differentially expressed genes and the 22 differentially upregulated genes in the IBA1^{HIGH} group showed an association with phagocytic pathways and the complement cascade, respectively, as well as immune-related pathways (Figure S4 and Tables S10–S13). The TCGA and Gravendeel datasets were employed to screen for changes in mRNA levels of 17,811 and 19,944 genes between the glioblastomas with the highest and lowest *CD204* mRNA levels. Interaction network analyses of the differentially upregulated genes from these two datasets confirmed the central role of *IL6* in CD204-enriched tumours. *CD204* itself clustered with genes related to collagen and extracellular matrix modelling. Further, KEGG and Reactome enrichment and pathway analyses of the *in*

silico datasets verified the functional profile of the CD204-enriched glioblastomas identified by NanoString (Figures S5 and S6 and Tables S14–S17).
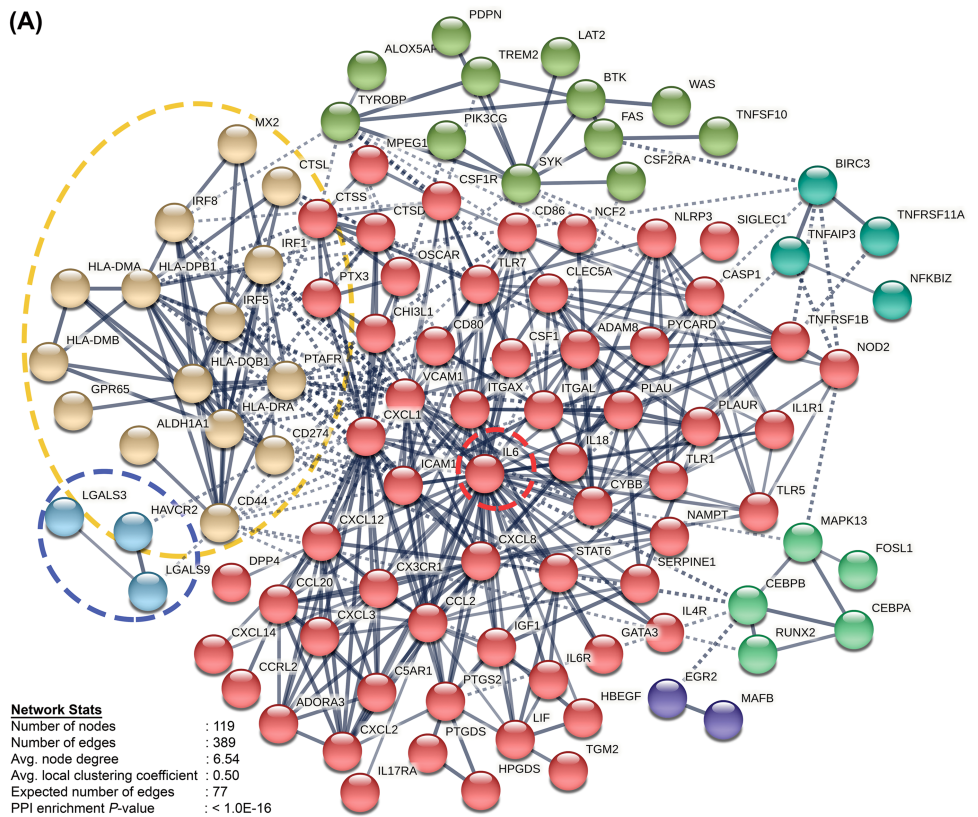
Validation of gene expression profile in CD204-enriched glioblastoma

The unique gene expression profile for CD204-enriched glioblastomas was corroborated by immunohistochemical analysis. Of the 46 glioblastoma samples, 10 were included from the CD204^{LOW}/IBA1^{LOW} group and 10 from the CD204^{HIGH} groups. A gene signature comprising 10 differentially upregulated genes was used for protein validation. The genes included in the signature were selected based on their fold-changes, connectivity levels in the interaction network analysis, level of gene matches in the pathway analyses, and antibody availability. Ultimately, protein expression was investigated for the following genes: *BIRC3*, *TNFAIP3*, *NOD2*, *IL6*, *ICAM1*, *CD44*, *PD-L1*, *GAL3*, *GAL9* and *TIM3*. STRING connectivity analysis was used to verify that the 10 genes as well as CD204 were able to form an interacting network with *IL6* in the epicentre (Figure 5E). The subgrouping of the 20 samples was verified by chromogenic staining for IBA1 and CD204 (Figure 6A,B). Immunostaining showed that BIRC3 was primarily localised in the nucleus (Figure 6C), but expression was also observed in the cytoplasm (not shown). TNFAIP3, NOD2, IL6, ICAM1, CD44, PD-L1 and GAL3 were expressed in the membrane and/or the cytoplasm, and expression levels seemed to depend on CD204 level being highest in CD204^{HIGH} glioblastomas (Figure 6D–J). When applying software-based algorithms, the area fractions were significantly higher in CD204^{HIGH} compared with CD204^{LOW}/IBA1^{LOW} tumours for IBA1 ($p < 0.01$), CD204 ($p < 0.001$), TNFAIP3 ($p < 0.01$), IL6 ($p < 0.001$), ICAM1 ($p < 0.01$), CD44 ($p < 0.01$) and GAL3 ($p < 0.05$) (Figure 6K). The same tendency was observed for NOD2 ($p = 0.075$), while no significant difference was found for BIRC3 ($p = 0.17$). GAL9$^+$ and TIM3$^+$ cells were also significantly more frequent in CD204^{HIGH} tumours ($p < 0.01$ or $p < 0.001$) (Figure 6L).

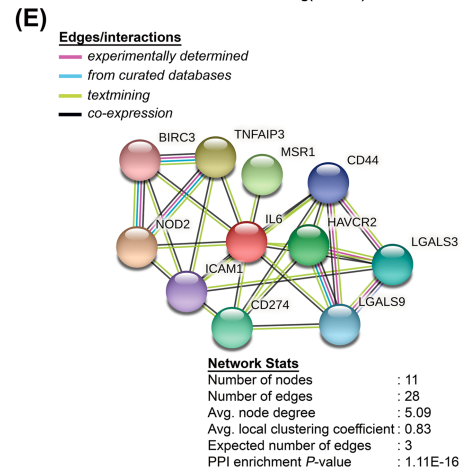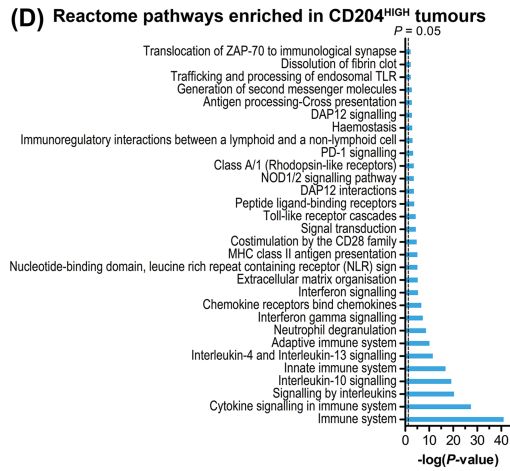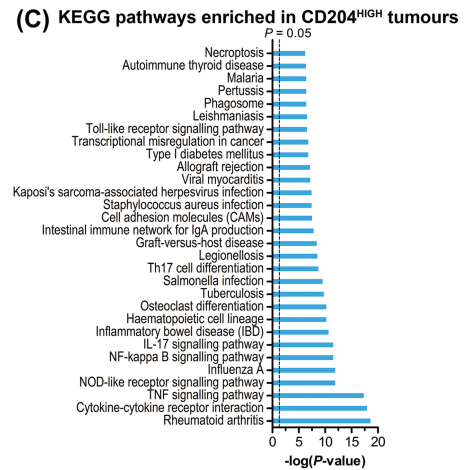## CD204 is an important prognostic factor and is associated with worse overall survival

A heatmap was generated for the 20 tumours based on the level of CD204, necrosis, cellularity and the eight significantly overexpressed proteins of 10-gene signature described above. Unsupervised hierarchical clustering revealed two major clusters (Figure 6M) similar to the pattern found in the NanoString transcriptome analysis. Cluster 1 was mostly characterised by CD204^{LOW} tumours, whereas Cluster 2 consisted solely of CD204^{HIGH} tumours. Kaplan–Meier estimator and log-rank testing showed a significant separation in overall survival between the two clusters (HR 2.92, $P = 0.044$) (Figure 6N). However, similar to the findings from the transcriptome analysis, the two clusters did not show greater prognostic impact compared with CD204 alone (HR 3.93, $P = 0.016$, Kaplan–Meier plot not shown). To further

FIGURE 5 STRING connectivity network and enrichment analysis of CD204-enriched glioblastomas. (A,B) The interaction network analysis was performed on the 119 genes that were uniquely upregulated in CD204-enriched glioblastomas. Clustering identified three major clusters and three minor clusters. The biggest cluster (red) centralised around *IL6*, which had the most interactions of all the genes (B) and connected to the other subnetworks either directly or indirectly via, for example, *ICAM1* and *PD-L1* [*CD274*]. (C,D) KEGG and Reactome enrichment analyses revealed that the differentially upregulated genes were especially involved cytokine signalling pathways including TNF, IL10, IL4/13, interferon as well as the NOD-like receptor and NF-kappa B signalling pathways. (E) Some of the upregulated genes were selected for protein and *in silico* mRNA validation. The selected genes formed a connectivity network which also centralised around *IL6*. Line annotations: thick = highest edge confidence (0.90), thin = high edge confidence (0.70); dotted = intercluster connections

FIGURE 6 Legend on next page.

FIGURE 6 Validation of selected upregulated genes in the CD204-enriched glioblastoma profile. (A,B) High levels of IBA1 and CD204 was confirmed by immunohistochemistry in the validation cohort consisting of 20 glioblastomas. (C) BIRC3 was expressed primarily in the nuclei, and its protein expression did not appear to be influenced by CD204 levels. (D) TNFAIP3 showed a cytoplasmic expression pattern which appeared more intense and widespread in glioblastomas with high CD204 levels. (E) NOD2 exhibited a diffuse cytoplasmic expression pattern and seemed to be expressed to a higher extent in CD204-enriched glioblastomas. (F) IL6 also showed a diffuse staining pattern, which seemed more pronounced in CD204-enriched glioblastomas. (G) ICAM1 was expressed in membrane of some of the glioblastomas, especially CD204-enriched glioblastomas. (H) CD44 was widely expressed in all tumours, but exhibited a more dense and intense staining pattern in CD204-enriched tumours. (I) PD-L1 was detected in the cytoplasm and membrane at low-moderate level in most tumours, but expression appeared more pronounced in CD204-enriched tumours. (J) GAL3 had a cytoplasmic expression pattern, but was rarely expressed in CD204-sparse tumours. (K) Software-based algorithms was used to quantify the expression level of the investigated proteins, and their overexpression in the CD204-enriched glioblastomas was validated for all but NOD2 and BIRC3. (L) TIM3 (purple) and GAL9 (yellow) expression was evaluated by double immunohistochemistry and cell counting. Both TIM3$^+$ and GAL9$^+$ cells were more frequent in CD204-enriched glioblastomas. (M) Data from the validated proteins, CD204 as well as necrotic level and cellularity was used to generate a heatmap and cluster analysis grouped most of the CD204-enriched into more cluster (Cluster 2). (N) The CD204-enriched cluster was associated with shorter overall survival. (O) Schematic illustration of the presumed cross-talk between glioblastoma cells and tumour-associated microglia/macrophages (TAMs) in CD204-enriched glioblastomas. Tumour-derived factors, for example, IL6, CXCL12, CSF1 and CCL2 attract brain-resident microglia and peripheral macrophages to the site of the tumour, while simultaneously activating and polarising the TAMs. The cross-talk between the glioblastoma cells and TAMs results in expression and secretion of different cytokines/chemokines or/and receptors, which promote tumour hypoxia, angiogenesis and matrix remodelling and influence immune checkpoint signalling. The tumour microenvironment in CD204-enriched glioblastoma may thus ultimately enable tumour growth, resistance and progression. *Inserts* in A–J show examples of the software-based algorithms. In L upwards and downwards arrows indicate double-positive cells (i.e., TIM3$^+$ GAL9$^+$ cells), rightwards arrows indicate GAL9$^+$ TIM3$^-$ cells, and leftwards arrows indicate TIM3$^+$ GAL9$^-$ cells. Horizontal and vertical lines indicate mean $\pm$ SEM. *$p < 0.05$; **$p < 0.01$; ***$p < 0.001$. *Scale bar* 50 μM. *Abbreviations:* BIRC3, baculoviral IAP repeat containing-3; *GAL3*, galectin-3; *GAL9*, galectin-9; *IBA1*, ionised calcium-binding adaptor molecule-1; *ICAM1*, intercellular adhesion molecule-1; *IL6*, interleukin-6; *NOD2*, nucleotide-binding oligomerisation domain-containing protein-2; *PD-L1*, programmed death-ligand 1; *TIM3*, T-cell immunoglobulin and mucin-domain containing-3; *TNFAIP3*, tumour necrosis factor, alpha-induced protein-3

examine the prognostic value of CD204-enriched glioblastomas, the TCGA and Gravendeel datasets were evaluated, and patients with glioblastoma were stratified based on the mRNA expression levels of *CD204* and *IBA1*. Survival analyses confirmed that high CD204 had a detrimental impact on survival (Figure S7A,B); in particular, patients with high CD204 and low IBA1 levels had a poorer prognosis (TCGA: HR 1.91, $p = 0.001$, and Gravendeel: 2.50, $p = 0.022$). The survival detriment was not potentiated when adjusting for mRNA expression of the eight genes from the 10-gene signature (TCGA: HR 2.02, $p = 0.001$, and Gravendeel: 2.37, $p = 0.047$) (Figure S7C).

DISCUSSION

In the present study, we demonstrated that perivascular and peri-necrotic areas were densely populated by IBA-1$^+$ and CD204$^+$ TAMs which co-localised with mainly PDPN$^+$ tumour cells, but to a certain extent also with nestin$^+$ and SOX2$^+$ tumour cells in the perivascular niche, overall suggesting a possible crosstalk between TAMs and dedifferentiated tumour cells with a stem cell-like phenotype. We have previously reported that CD204 was a negative prognostic biomarker in high-grade glioma, including glioblastoma, favouring tumour progression [32]. Here, we performed mRNA transcriptome profiling of CD204-enriched glioblastomas using the NanoString digital barcode technology on FFPE tissue samples, which offers direct multi-plexed detection of RNA targets without amplification and with a high level of reproducibility and robustness [42–44]. We identified genes (e.g., *CCL2*, *CXCL12*, *IL6*, *ICAM1*, *TNFAIP3* and *PD-L1*) that were specif-ically upregulated in CD204-enriched tumours compared to

glioblastomas with low levels of TAMs, especially CD204$^+$ TAMs. We selected some of these genes and validated their expression using immunohistochemistry and by performing *in silico* mRNA analyses.

We performed transcriptome profiling of 46 glioblastomas with either high or low CD204 protein expression levels, and unsupervised clustering grouped the glioblastomas into two clusters. One cluster (Cluster 2)— which contained most of the CD204-enriched glioblastomas—correlated with shorter overall survival and was characterised by enrichment of multiple pathways especially the TNF and NOD-like receptor signalling pathways, which regulate immune response, apoptosis and shaping of the extracellular matrix [67, 68]. Consistent with previous studies [38, 39], our profiling of CD204-enriched glioblastomas revealed upregulation of genes belonging to all macrophage/microglia polarisation states: M1 (*CD86*, *CD80*, *IRF1*, *IL15RA* and *PTGS2*), M2/M2c (e.g., *TLR5*, *CXCL12*, *CD204*, *CCL2*, *IRF5*, *HLA*-genes and *IRF8*), and M0 (*GATA3* and *CD206*). Similar results have been found in recent studies using the single-cell RNA-sequencing and CyTOF techniques [40, 69]. This altogether suggests that the myeloid immune composition in brain tumours is highly het-erogeneous, and single-cell profiling has shown that this heterogene-ity is disease-, ontogenetic- and spatiotemporal-dependent [69–71].

In agreement with previous reports, we observed that both TAMs and dedifferentiated/stem-like glioblastoma cells accumulate [20–23, 37] and tend to co-reside [24, 26] in areas surrounding vasculature and necrosis/hypoxic niches. However, to our knowledge, we are the first to systemically perform a proximity study using a panel of seven markers related to cancer stemness and TAM markers. Our results showed that especially CD204$^+$ TAMS and PDPN$^+$ dedifferentiated tumour cells co-resided in these niches. Reportedly, the tumour cells

attract TAMs to the tumour sites by secreting, for example, CSF1, CCL2, CXCL12 and IL6 while simultaneously inducing an immunosuppressive TAM phenotype [24, 26, 28, 29] which in turn enhances tumour invasiveness in an autocrine and paracrine manner [24, 25]. Of the stem-like cell-related markers included in our NanoString panel, only PDPN, CD44 and ALDH1A1 were differentially upregulated in CD204-enriched glioblastoma. These genes have been linked to hypoxia [72, 73], radio-chemoresistance [14, 74, 75] and invasiveness through the actions of matrix metalloproteases (MMPs) and metalloprotease-disintegrins (ADAMs) [75–78]. Tumour hypoxia constitutes one of the cancer hallmarks and is associated with treatment resistance and angiogenesis [79], as well as an aggressive nature of glioblastoma [17, 80, 81] promoting migration [82], invasion and a mesenchymal shift [12, 23, 81]. To further investigate the possible relation between TAMs and tumour hypoxia, we investigated if the presence of necrosis correlated with the number of TAMs. We found that CD204-enriched glioblastomas had the highest level of necrosis. This finding is consistent with the nature of CD204 as CD204 belongs to the pattern recognition/scavenger receptor family and is known to phagocytise several ligands including apoptotic cells, collagen, low-density lipoproteins and myelin [73, 74]. In contrast, we observed that the overall tumour cellularity/cell density was lower in CD204-enriched glioblastoma relative to glioblastoma with low levels of TAMs. Interestingly, in cancer cell lines including the glioblastoma cell line U87-MG, cells grown at low cell density were reported to exhibit higher invasive capacity in vitro compared with cells grown at high density [83]. This effect was partly mediated through the Hippo and CXCR2 signalling pathways, and low-density cells showed an upregulation of several genes including the pro-angiogenic chemokines CXCL1, CXCL2, CXCL3 and CXCL8 [84, 85], as well as IL6 and CD44 [83]. Further, in oesophageal cancer, the response to neo-adjuvant chemotherapy was influenced by the tumour cell density found in the pre-chemo biopsy being poorest in patients with the lowest and highest density levels [86]. Collectively, these results suggest that CD204$^+$ TAMs thrive in hypoxic niches and may facilitate the formation of a pro-invasive, resistant and dedifferentiated phenotype of glioblastoma.

Our differential expression analysis showed that several chemokines (CCL2, CCL20, CXCL1, CXCL2, CXCL3, CXCL8, CXCL12, CXCL14 and CCRL2) and cytokines (CSF1, IL6, LIF, IL4I1 and IL18) were uniquely upregulated in CD204-enriched glioblastomas, especially CCL20, IL6, CXCL8 and CXCL14. By binding to their respective receptors, these molecules promote myeloid infiltration, immune evasion, hypoxia, angiogenesis, proliferation, migration/invasion, mesenchymal transition and progression in glioblastoma [11, 84, 87–91]. We identified IL6 as an integral player in the inflammatory environment of CD204-enriched glioblastomas by performing connectivity analysis of the differentially upregulated genes, and we confirmed its upregulation at a protein level using immunohistochemistry. We also investigated the protein expression of genes that interacted either directly or indirectly with IL6, and we were able to validate the over-expression of TNFAIP3, ICAM1, CD44 and GAL3 as well as the co-inhibitory immune checkpoint molecules PD-L1, GAL9 and TIM3 in

glioblastomas with high CD204 levels. NOD2 expression tended to positively correlate with CD204 as well, while BIRC3 expression was CD204-independent possibly due to posttranscriptional down-regulation [92]. Similar to the transcriptome data, clustering of the overexpressed proteins identified two clusters. One cluster (Cluster 2)—which contained most of the CD204-enriched glioblastomas—predicted an unfavourable patient outcome, but the cluster was not a stronger prognosticator of survival than CD204 alone. As recently reported by Yuan et al. [41], we also found that high CD204 levels correlated with expression of the immune checkpoint markers PD-L1, TIM3 and GAL9, which suggests a possible synergy between CD204 and promotion of exhausted T cells [30, 46]. Interestingly, inhibition of CD204 in dendritic cells (DC) enhanced the efficacy of a DC vaccine in a melanoma model by restoring the T cell response and anti-tumour immunity [93]. Similarly, in an ovarian cancer model, administration of CD204-targeted immunotoxin substantially inhibited tumour burden and reduced the amount of suppressive vascular leukocytes [94]. Summarised, our findings suggest that CD204-enriched glioblastomas are associated with a highly inflamed TME, which produces several molecules such as IL6 that can facilitate progression. Further, CD204 may have an immunoregulatory function that could mediate immune evasion (Figure 6O).

IL6 is an essential regulator of innate and acquired immunity. In cancer, it is considered one of the major tumour-promoting cytokines and is produced by both neoplastic and non-neoplastic cells [95, 96]. IL6 stimulates expression of adhesion molecules and chemokines such as ICAM1, vascular cell adhesion protein-1 (VCAM1) and CCL2 [97], which in turn promote tumourigenesis and tumour-driven inflammation through multiple signalling pathways including interferon, Jak-STAT and NF-kappa B [84, 95, 96, 98–100]. In glioblastoma, IL6 is especially expressed by TAMs and endothelial cells, while its receptor IL6R is expressed to a higher extent by glioma cells [27, 33, 101–103]. Reportedly, TNFAIP3 and GAL3 are hypoxia-driven and NF-kappa B-dependent genes involved in regulation of apoptosis [104–106] promoting cell survival [107, 108], cancer stemness/dedifferentiation, tumour growth [107] and possibly chemoresistance [109]. Interestingly, GAL3 was reported to be expressed by microglia only in neoplastic brain tissue [110] and was associated with the myelination/remyelination process as activated GAL3$^+$ microglia were able to engulf and internalise myelin-debris [111, 112] suggesting that GAL3 may act in concert with MMPs as well as CD204 in the matrix remodelling process. ICAM1 and CD44 are both associated with tumour hypoxia, treatment resistance [113], as well migration/invasion and matrix remodelling [114, 115] and were found to correlate with PD-L1 expression [116]. A previous study reported that PD-L1 is a direct target of hypoxia-inducible factor 1-alpha (HIF1A), and inhibition of PD-L1 during hypoxia augmented myeloid-derived suppressor cell (MDSC)-mediated T cell activation and reduced MDSC-derived IL6 and IL10 in vitro [117]. In turn, glioblastoma-derived IL6 was reported to induce PD-L1 expression on myeloid cells and promote apoptosis of CD8$^+$ T cells, overall promoting immunosuppression [118]. In glioblastoma xenografts, depletion or inhibition of IL6, its receptor IL6R, or endothelial-produced IL6 by short hair RNA or an

IL6 antibody reduced glioma growth and prolonged overall survival in mice [27, 102, 103, 118, 119], and the anti-tumour activity was potentiated when combining with an immune checkpoint antibody against programmed death-1 (PD-1) [118] or the anti-angiogenetic antibody bevacizumab [119]. Overall, these data suggest that IL6 is an important player in CD204-enriched glioblastoma, correlates with an aggressive tumour profile, and may be a candidate for targeted treatment in glioblastoma. Several anti-IL6 therapeutics (targeting either IL6/IL6R or downstream signalling molecules, e.g., Jak and STAT) are already used or in the pipeline for treatment of connective tissue disorders and myeloproliferative diseases [96].

In recent years, the interest in targeting myeloid cells (i.e., TAMs and MDSCs) has increased as a means of enhancing the anti-glioma response of standard treatment [95, 120–122]. One of the therapeutic strategies is re-education or elimination of TAMs by blockade of key chemokine/cytokine signalling pathways including the CCL2-CCR2 [123], CXCL2/8-CXCR2 [124, 125] and CSF1-CSF1R [126, 127] axes. This approach has shown great promise *in vivo*. However, administration of the anti-CSF1R antibody PLX3397 showed no efficacy in a phase II clinical trial with recurrent glioblastoma patients [128] possibly due to the innate self-renewing ability of microglia ensuring rapid recolonisation within the brain [129] and tumour-derived survival factors [130]. These findings underscore the importance of the bidirectional crosstalk between tumour cells and the microenvironment, in which the tumour grows and evolves. Deeper insight into the spatiotemporal dynamics of TAMs and the tumour immune microenvironment in general is necessary to achieve efficient immunotherapies including those directed against TAMs. The results of our study suggest that a future therapeutic strategy could be repolarisation of TAMs into an anti-tumourigenic phenotype by targeting CD204 and/or IL6 using, for example, neutralising antibodies. This strategy could especially be relevant in patients whose tumours express high levels of CD204 and/or IL6 at time of diagnosis, thus possibly serving as predictive and prognostic biomarkers.

In conclusion, our findings show that TAMs including CD204$^+$ TAMs accumulate in perivascular and perinecrotic/hypoxic niches in close proximity to dedifferentiated/stem-like glioblastoma cells. Gene profiling revealed that CD204-enriched glioblastoma differentially expressed markers related to the entire M0–M2 spectrum. Pathway and connectivity analyses demonstrated that CD204-enriched glioblastomas were associated with an inflamed phenotype. This phenotype correlated with poor prognosis and expressed high levels of several pro-tumourigenic factors especially IL6. These results highlight the importance of CD204 in the glioblastoma microenvironment and suggest that CD204 is a possible immunoregulatory molecule which could serve as a valuable target in combined immunotherapy.

ACKNOWLEDGEMENTS

CONFLICT OF INTEREST

Both authors declare that they have no conflicts of interest.

AUTHOR CONTRIBUTIONS

M. D. S. and B. W. K. conceived the study and designed the experiments. M. D. S. collected, assembled, analysed the data, and interpreted the results. B. W. K. contributed with the reagents/materials/analysis tools. MDS drafted and edited the manuscript. Both authors have read and approved the final manuscript.

FUNDING INFORMATION

ETHICS STATEMENT

Study approval was obtained from by the Regional Scientific Ethical Committee of the Region of Southern Denmark (Project-ID: S-20150148) and the Danish Data Protection Authority (file number: 16/11065). The use of tissue was permitted by all patients in the Danish Tissue Application Register. The study was performed in agreement with the Declaration of Helsinki.

PEER REVIEW

The peer review history for this article is available at https://publons.com/publon/10.1111/nan.12772.

DATA AVAILABILITY STATEMENT

The data that supports the findings of this study are available either in the supplementary material of this article or from the corresponding author upon reasonable request.

ORCID

Mia D. Sørensen 🔟 https://orcid.org/0000-0002-0105-2940

REFERENCES

1. Louis DN, Ohgaki H, Wiestler OD, et al. *WHO Classification of Tumours of the Central Nervous System, Revised*. 4thed. Lyon: International Agency for Research on Cancer (IARC); 2016.
2. Ostrom QT, Gittleman H, Xu J, et al. CBTRUS statistical report: primary brain and other central nervous system tumors diagnosed in the United States in 2009–2013. *Neuro-Oncol*. 2016;18(suppl_5): v1-v75.

3. Stupp R, Mason WP, van den Bent MJ, et al. Radiotherapy plus concomitant and adjuvant temozolomide for glioblastoma. *N Engl J Med*. 2005;352(10):987-996.

4. Stupp R, Hegi ME, Mason WP, et al. Effects of radiotherapy with concomitant and adjuvant temozolomide versus radiotherapy alone on survival in glioblastoma in a randomised phase III study: 5-year analysis of the EORTC-NCIC trial. *Lancet Oncol*. 2009;10: 459-466.

5. Patel AP, Tirosh I, Trombetta JJ, et al. Single-cell RNA-seq highlights intratumoral heterogeneity in primary glioblastoma. *Science*. 2014; 344:1396-1401.

6. Sottoriva A, Spiteri I, Piccirillo SGM, et al. Intratumor heterogeneity in human glioblastoma reflects cancer evolutionary dynamics. *Proc Natl Acad Sci*. 2013;110(10):4009-4014.

7. Phillips HS, Kharbanda S, Chen R, et al. Molecular subclasses of high-grade glioma predict prognosis, delineate a pattern of disease progression, and resemble stages in neurogenesis. *Cancer Cell*. 2006; 9(3):157-173.

8. Brennan CW, Verhaak RG, McKenna A, et al. The somatic genomic landscape of glioblastoma. *Cell*. 2013;155:462-477.

9. Neftel C, Laffy J, Filbin MG, et al. An integrative model of cellular states, plasticity, and genetics for glioblastoma. *Cell*. 2019;178: 835-849.

10. Charles NA, Holland EC, Gilbertson R, Glass R, Kettenmann H. The brain tumor microenvironment. *Glia*. 2011;59(8):1169-1180.

11. Chen W, Xia T, Wang D, et al. Human astrocytes secrete IL-6 to promote glioma migration and invasion through upregulation of cytomembrane MMP14. *Oncotarget*. 2016;7(38):62425-62438.

12. Joseph JV, Conroy S, Pavlov K, et al. Hypoxia enhances migration and invasion in glioblastoma by promoting a mesenchymal shift mediated by the HIF1alpha-ZEB1 axis. *Cancer Lett*. 2015;359(1): 107-116.

13. Tomaszewski W, Sanchez-Perez L, Gajewski TF, Sampson JH. Brain tumor microenvironment and host state: implications for immunotherapy. *Clin Cancer Res: Off J Am Assoc Cancer Res*. 2019;25(14): 4202-4210.

14. Bhat KP, Balasubramaniyan V, Vaillant B, et al. Mesenchymal differentiation mediated by NF-κB promotes radiation resistance in glioblastoma. *Cancer Cell*. 2013;24(3):331-346.

15. Sarkaria JN, Kitange GJ, James CD, et al. Mechanisms of chemoresistance to alkylating agents in malignant glioma. *Clin Cancer Res: Off J Am Assoc Cancer Res*. 2008;14(10):2900-2908.

16. Piao Y, Liang J, Holmes L, et al. Glioblastoma resistance to anti-VEGF therapy is associated with myeloid cell infiltration, stem cell accumulation, and a mesenchymal phenotype. *Neuro-Oncol*. 2012;14(11): 1379-1392.

17. Beier D, Schulz JB, Beier CP. Chemoresistance of glioblastoma cancer stem cells—much more complex than expected. *Mol Cancer*. 2011;10(1):128.

18. Schonberg DL, Lubelski D, Miller TE, Rich JN. Brain tumor stem cells: molecular characteristics and their impact on therapy. *Mol Asp Med*. 2013;39:82-101.

19. Filatova A, Acker T, Garvalov BK. The cancer stem cell niche(s): the crosstalk between glioma stem cells and their microenvironment. *Biochim Biophys Acta*. 1830;2013(2):2496-2508.

20. Aderetti DA, Hira VVV, Molenaar RJ, van Noorden CJF. The hypoxic peri-arteriolar glioma stem cell niche, an integrated concept of five types of niches in human glioblastoma. *Biochim Biophys Acta Rev Cancer*. 1869;2018(2):346-354.

21. Calabrese C, Poppleton H, Kocak M, et al. A perivascular niche for brain tumor stem cells. *Cancer Cell*. 2007;11(1):69-82.

22. Hira VV, Ploegmakers KJ, Grevers F, et al. CD133^{+} and Nestin^{+} glioma stem-like cells reside around CD31^{+} arterioles in niches that express SDF-1alpha, CXCR4, osteopontin and cathepsin K. *J Histochem Cytochem*. 2015;63(7):481-493.

23. Heddleston JM, Li Z, McLendon RE, Hjelmeland AB, Rich JN. The hypoxic microenvironment maintains glioblastoma stem cells and promotes reprogramming towards a cancer stem cell phenotype. *Cell Cycle*. 2009;8:3274-3284.

24. Yi L, Xiao H, Xu M, et al. Glioma-initiating cells: a predominant role in microglia/macrophages tropism to glioma. *J Neuroimmunol*. 2011; 232(1-2):75-82.

25. Ye XZ, Xu SL, Xin YH, et al. Tumor-associated microglia/macrophages enhance the invasion of glioma stem-like cells via TGF-beta1 signaling pathway. *J Immunol*. 2012;189:444-453.

26. Wang SC, Hong JH, Hsueh C, Chiang CS. Tumor-secreted SDF-1 promotes glioma invasiveness and TAM tropism toward hypoxia in a murine astrocytoma model. *Lab Invest: J Tech Methods Pathol*. 2012; 92:151-162.

27. Dzaye OD, Hu F, Derkow K, et al. Glioma stem cells but not bulk glioma cells upregulate IL-6 secretion in microglia/brain macrophages via Toll-like receptor 4 signaling. *J Neuropathol Exp Neurol*. 2016; 75(5):429-440.

28. Wu A, Wei J, Kong LY, et al. Glioma cancer stem cells induce immunosuppressive macrophages/microglia. *Neuro-Oncol*. 2010;12(11): 1113-1125.

29. Gabrusiewicz K, Li X, Wei J, et al. Glioblastoma stem cell-derived exosomes induce M2 macrophages and PD-L1 expression on human monocytes. *Onco Targets Ther*. 2018;7(4):e1412909.

30. Binnewies M, Roberts EW, Kersten K, et al. Understanding the tumor immune microenvironment (TIME) for effective therapy. *Nat Med*. 2018;24(5):541-550.

31. Graeber MB, Scheithauer BW, Kreutzberg GW. Microglia in brain tumors. *Glia*. 2002;40(2):252-259.

32. Sorensen MD, Dahlrot RH, Boldt HB, Hansen S, Kristensen BW. Tumour-associated microglia/macrophages predict poor prognosis in high-grade gliomas and correlate with an aggressive tumour subtype. *Neuropathol Appl Neurobiol*. 2018;44(2):185-206.

33. Li W, Graeber MB. The molecular profile of microglia under the influence of glioma. *Neuro-Oncology*. 2012;14(8):958-978.

34. Sielska M, Przanowski P, Wylot B, et al. Distinct roles of CSF family cytokines in macrophage infiltration and activation in glioma progression and injury response. *J Pathol*. 2013;230(3):310-321.

35. Komohara Y, Ohnishi K, Kuratsu J, Takeya M. Possible involvement of the M2 anti-inflammatory macrophage phenotype in growth of human gliomas. *J Pathol*. 2008;216(1):15-24.

36. Lisi L, Stigliano E, Lauriola L, Navarra P, Dello RC. Proinflammatory-activated glioma cells induce a switch in microglial polarization and activation status, from a predominant M2b phenotype to a mixture of M1 and M2a/B polarized cells. *ASN Neuro*. 2014;6(3):171-183.

37. Zeiner PS, Preusse C, Golebiewska A, et al. Distribution and prognostic impact of microglia/macrophage subpopulations in gliomas. *Brain Pathol*. 2018;29(4):513-529.

38. Szulzewsky F, Pelz A, Feng X, et al. Glioma-associated microglia/macrophages display an expression profile different from M1 and M2 polarization and highly express Gpnmb and Spp1. *PLoS ONE*. 2015;10(2):e0116644.

39. Gabrusiewicz K, Rodriguez B, Wei J, et al. Glioblastoma-infiltrated innate immune cells resemble M0 macrophage phenotype. *JCI Insight*. 2016;1(2).

40. Muller S, Kohanbash G, Liu SJ, et al. Single-cell profiling of human gliomas reveals macrophage ontogeny as a basis for regional differences in macrophage activation in the tumor microenvironment. *Genome Biol*. 2017;18(1):234.

41. Yuan Y, Zhao Q, Zhao S, et al. Characterization of transcriptome profile and clinical features of a novel immunotherapy target CD204 in diffuse glioma. *Cancer Med*. 2019;8(8):3811-3821.

42. Veldman-Jones MH, Brant R, Rooney C, et al. Evaluating robustness and sensitivity of the NanoString technologies nCounter platform to

enable multiplexed gene expression analysis of clinical samples. *Cancer Res*. 2015;75(13):2587-2593.

43. Reis PP, Waldron L, Goswami RS, et al. mRNA transcript quantification in archival samples using multiplexed, color-coded probes. *BMC Biotechnol*. 2011;11(1):46.

44. Goytain A, Ng T. NanoString nCounter technology: high-throughput RNA validation. *Methods Mol Biol*. 2020;2079:125-139.

45. Dahlrot RH, Kristensen BW, Hjelmborg J, Herrstedt J, Hansen S. A population-based study of high-grade gliomas and mutated isocitrate dehydrogenase 1. *Int J Clin Exp Pathol*. 2013;6(1):31-40.

46. Baumeister SH, Freeman GJ, Dranoff G, Sharpe AH. Coinhibitory pathways in immunotherapy for cancer. *Annu Rev Immunol*. 2016; 34(1):539-573.

47. Ravindran S, Rasool S, Maccalli C. The cross talk between cancer stem cells/cancer initiating cells and tumor microenvironment: the missing piece of the puzzle for the efficient targeting of these cells with immunotherapy. *Cancer Microenviron*. 2019;12(2-3):133-148.

48. Rasper M, Schafer A, Piontek G, et al. Aldehyde dehydrogenase 1 positive glioblastoma cells show brain tumor stem cell capacity. *Neuro-Oncology*. 2010;12(10):1024-1033.

49. Leonetti C, Biroccio A, Graziani G, Tentori L. Targeted therapy for brain tumours: role of PARP inhibitors. *Curr Cancer Drug Targets*. 2012;12(3):218-236.

50. Zhu C, Chen X, Guan G, et al. IFI30 is a novel immune-related target with predicting value of prognosis and treatment response in glioblastoma. *Onco Targets Ther*. 2020;13:1129-1143.

51. Metz P, Reuter A, Bender S, Bartenschlager R. Interferon-stimulated genes and their role in controlling hepatitis C virus. *J Hepatol*. 2013; 59(6):1331-1341.

52. Tiwari R, de la Torre JC, McGavern DB, Nayak D. Beyond tethering the viral particles: immunomodulatory functions of tetherin (BST-2). *DNA Cell Biol*. 2019;38(11):1170-1177.

53. Kreth S, Heyn J, Grau S, Kretzschmar HA, Egensperger R, Kreth FW. Identification of valid endogenous control genes for determining gene expression in human glioma. *Neuro-Oncology*. 2010;12(6):570-579.

54. Grube S, Göttig T, Freitag D, Ewald C, Kalff R, Walter J. Selection of suitable reference genes for expression analysis in human glioma using RT-qPCR. *J Neuro-Oncol*. 2015;123(1):35-42.

55. Ito D, Imai Y, Ohsawa K, Nakajima K, Fukuuchi Y, Kohsaka S. Microglia-specific localisation of a novel calcium binding protein, Iba1. *Brain Res Mol Brain Res*. 1998;57(1):1-9.

56. Ramachandran RK, Sorensen MD, Aaberg-Jessen C, Hermansen SK, Kristensen BW. Expression and prognostic impact of matrix metalloproteinase-2 (MMP-2) in astrocytomas. *PLoS ONE*. 2017; 12(2):e0172234.

57. Bowman RL, Wang Q, Carro A, Verhaak RG, Squatrito M. GlioVis data portal for visualization and analysis of brain tumor expression datasets. *Neuro-Oncology*. 2017;19(1):139-141.

58. The Cancer Genome Atlas Research Network. Comprehensive genomic characterization defines human glioblastoma genes and core pathways. *Nature*. 2008;455(7216):1061-1068.

59. Gravendeel LA, Kouwenhoven MC, Gevaert O, et al. Intrinsic gene expression profiles of gliomas are a better predictor of survival than histology. *Cancer Res*. 2009;69(23):9065-9072.

60. Benjamini Y, Yekutieli D. The control of the false discovery rate in multiple testing under dependency. *Ann Stat*. 2001;29(4):1165-1188.

61. Szklarczyk D, Gable AL, Lyon D, et al. STRING v11: protein–protein association networks with increased coverage, supporting functional discovery in genome-wide experimental datasets. *Nucleic Acids Res*. 2019;47(D1):D607-D613.

62. Brohée S, van Helden J. Evaluation of clustering algorithms for protein–protein interaction networks. *BMC Bioinformatics*. 2006; 7(1):1-9.

63. Babicki S, Arndt D, Marcu A, et al. Heatmapper: web-enabled heat mapping for all. *Nucleic Acids Res*. 2016;44(W1):W147-W153.

64. Sica A, Schioppa T, Mantovani A, Allavena P. Tumour-associated macrophages are a distinct M2 polarised population promoting tumour progression: potential targets of anti-cancer therapy. *Eur J Cancer*. 2006;42:717-727.

65. Mantovani A, Sica A, Sozzani S, Allavena P, Vecchi A, Locati M. The chemokine system in diverse forms of macrophage activation and polarization. *Trends Immunol*. 2004; 25(12):677-686.

66. Hao N-B, Lü M-H, Fan Y-H, Cao Y-L, Zhang Z-R, Yang S-M. Macrophages in tumor microenvironments and the progression of tumors. *Clin Dev Immunol*. 2012;2012:948098.

67. Balkwill F. Tumour necrosis factor and cancer. *Nat Rev Cancer*. 2009; 9(5):361-371.

68. Velloso FJ, Trombetta-Lima M, Anschau V, Sogayar MC, Correa RG. NOD-like receptors: major players (and targets) in the interface between innate immunity and cancer. *Biosci Rep*. 2019;39(4): BSR20181709.

69. Sankowski R, Böttcher C, Masuda T, et al. Mapping microglia states in the human brain through the integration of high-dimensional techniques. *Nat Neurosci*. 2019;22(12):2098-2110.

70. Masuda T, Sankowski R, Staszewski O, et al. Spatial and temporal heterogeneity of mouse and human microglia at single-cell resolution. *Nature*. 2019;566(7744):388-392.

71. Friebel E, Kapolou K, Unger S, et al. Single-cell mapping of human brain cancer reveals tumor-specific instruction of tissue-invading leukocytes. *Cell*. 2020;181:1626-1642.

72. Soehngen E, Schaefer A, Koeritzer J, et al. Hypoxia upregulates aldehyde dehydrogenase isoform 1 (ALDH1) expression and induces functional stem cell characteristics in human glioblastoma cells. *Brain Tumor Pathol*. 2014;31(4):247-256.

73. Mishima K, Kato Y, Kaneko MK, Nishikawa R, Hirose T, Matsutani M. Increased expression of podoplanin in malignant astrocytic tumors as a novel molecular marker of malignant progression. *Acta Neuropathol*. 2006;111(5):483-488.

74. Schafer A, Teufel J, Ringel F, et al. Aldehyde dehydrogenase 1A1—a new mediator of resistance to temozolomide in glioblastoma. *Neuro-Oncology*. 2012;14(12):1452-1464.

75. Dong F, Eibach M, Bartsch JW, et al. The metalloprotease-disintegrin ADAM8 contributes to temozolomide chemoresistance and enhanced invasiveness of human glioblastoma cells. *Neuro-Oncology*. 2015;17(11):1474-1485.

76. Xu SL, Liu S, Cui W, et al. Aldehyde dehydrogenase 1A1 circumscribes high invasive glioma cells and predicts poor prognosis. *Am J Cancer Res*. 2015;5(4):1471-1483.

77. Wicki A, Christofori G. The potential role of podoplanin in tumour invasion. *Br J Cancer*. 2007;96(1):1-5.

78. Nishikawa M, Inoue A, Ohnishi T, et al. Significance of glioma stem-like cells in the tumor periphery that express high levels of CD44 in tumor invasion, early progression, and poor prognosis in glioblastoma. *Stem Cells Int*. 2018;2018:5387041.

79. Kucharzewska P, Christianson HC, Welch JE, et al. Exosomes reflect the hypoxic status of glioma cells and mediate hypoxia-dependent activation of vascular cells during tumor development. *Proc Natl Acad Sci U S A*. 2013;110(18):7312-7317.

80. Brat DJ, Castellano-Sanchez AA, Hunter SB, et al. Pseudopalisades in glioblastoma are hypoxic, express extracellular matrix proteases, and are formed by an actively migrating cell population. *Cancer Res*. 2004;64(3):920-927.

81. Xu H, Rahimpour S, Nesvick CL, et al. Activation of hypoxia signaling induces phenotypic transformation of glioma cells: implications for bevacizumab antiangiogenic therapy. *Oncotarget*. 2015;6(14): 11882-11893.

82. Li P, Zhou C, Xu L, Xiao H. Hypoxia enhances stemness of cancer stem cells in glioblastoma: an in vitro study. *Int J Med Sci*. 2013;10(4): 399-407.

83. Sharif GM, Schmidt MO, Yi C, et al. Cell growth density modulates cancer cell vascular invasion via Hippo pathway activity and CXCR2 signaling. *Oncogene*. 2015;34(48):5879-5889.

84. Groblewska M, Litman-Zawadzka A, Mroczko B. The role of selected chemokines and their receptors in the development of gliomas. *Int J Mol Sci*. 2020;21(10).

85. Balkwill FR. The chemokine system and cancer. *J Pathol*. 2012; 226(2):148-157.

86. Hale MD, Nankivell MG, Mueller W, et al. The relationship between tumor cell density in the pretreatment biopsy and survival after chemotherapy in OE02 trial esophageal cancer patients. *J Clin Oncol*. 2014;32:49-49.

87. Mantovani A, Allavena P, Sozzani S, Vecchi A, Locati M, Sica A. Chemokines in the recruitment and shaping of the leukocyte infiltrate of tumors. *Semin Cancer Biol*. 2004;14(3):155-160.

88. Wang L, Qin H, Li L, et al. Overexpression of CCL20 and its receptor CCR6 predicts poor clinical prognosis in human gliomas. *Med Oncol*. 2012;29(5):3491-3497.

89. Jung Y, Ahn SH, Park H, et al. MCP-1 and MIP-3α secreted from necrotic cell-treated glioblastoma cells promote migration/infiltration of microglia. *Cell Physiol Biochem*. 2018;48(3):1332-1346.

90. Chen Z, Mou L, Pan Y, Feng C, Zhang J, Li J. CXCL8 promotes glioma progression by activating the JAK/STAT1/HIF-1α/snail signaling axis. *Onco Targets Ther*. 2019;12:8125-8138.

91. Yin F, Xu Z, Wang Z, et al. Elevated chemokine CC-motif receptor-like 2 (CCRL2) promotes cell migration and invasion in glioblastoma. *Biochem Biophys Res Commun*. 2012;429(3-4):168-172.

92. Conze DB, Albert L, Ferrick DA, et al. Posttranscriptional down-regulation of c-IAP2 by the ubiquitin protein ligase c-IAP1 in vivo. *Mol Cell Biol*. 2005;25(8):3348-3356.

93. Yi H, Guo C, Yu X, et al. Targeting the immunoregulator SRA/CD204 potentiates specific dendritic cell vaccine-induced T-cell response and antitumor immunity. *Cancer Res*. 2011;71(21):6611-6620.

94. Bak SP, Walters JJ, Takeya M, Conejo-Garcia JR, Berwin BL. Scavenger receptor-A-targeted leukocyte depletion inhibits peritoneal ovarian tumor progression. *Cancer Res*. 2007;67(10):4783-4789.

95. Crusz SM, Balkwill FR. Inflammation and cancer: advances and new agents. *Nat Rev Clin Oncol*. 2015;12(10):584-596.

96. Garbers C, Heink S, Korn T, Rose-John S. Interleukin-6: designing specific therapeutics for a complex cytokine. *Nat Rev Drug Discov*. 2018;17(6):395-412.

97. Jones SA. Directing transition from innate to acquired immunity: defining a role for IL-6. *J Immunol*. 2005;175:3463-3468.

98. Jin X, Kim SH, Jeon HM, et al. Interferon regulatory factor 7 regulates glioma stem cells via interleukin-6 and Notch signalling. *Brain: J Neurol*. 2012;135(4):1055-1069.

99. McFarland BC, Hong SW, Rajbhandari R, et al. NF-κB-induced IL-6 ensures STAT3 activation and tumor aggressiveness in glioblastoma. *PLoS ONE*. 2013;8(11):e78728.

100. West AJ, Tsui V, Stylli SS, et al. The role of interleukin-6-STAT3 signalling in glioblastoma. *Oncol Lett*. 2018;16(4):4095-4104.

101. Chang CY, Li MC, Liao SL, Huang YL, Shen CC, Pan HC. Prognostic and clinical implication of IL-6 expression in glioblastoma multiforme. *J Clin Neurosci: Off J Neurosurg Soc Australasia*. 2005; 12(8):930-933.

102. Wang Q, He Z, Huang M, et al. Vascular niche IL-6 induces alternative macrophage activation in glioblastoma through HIF-2α. *Nat Commun*. 2018;9(1):1-5.

103. Wang H, Lathia JD, Wu Q, et al. Targeting interleukin 6 signaling suppresses glioma stem cell survival and tumor growth. *Stem Cells*. 2009;27:2393-2404.

104. Beyaert R, Heyninck K, Van Huffel S. A20 and A20-binding proteins as cellular inhibitors of nuclear factor-kappa B-dependent gene expression and apoptosis. *Biochem Pharmacol*. 2000;60(8): 1143-1151.

105. Murat A, Migliavacca E, Hussain SF, et al. Modulation of angiogenic and inflammatory response in glioblastoma by hypoxia. *PLoS ONE*. 2009;4(6):e5947.

106. Nakahara S, Oka N, Raz A. On the role of galectin-3 in cancer apoptosis. *Apoptosis*. 2005;10(2):267-275.

107. Hjelmeland AB, Wu Q, Wickman S, et al. Targeting A20 decreases glioma stem cell survival and tumor growth. *PLoS Biol*. 2010;8(2): e1000319.

108. Ikemori RY, Machado CM, Furuzawa KM, et al. Galectin-3 up-regulation in hypoxic and nutrient deprived microenvironments promotes cell survival. *PLoS ONE*. 2014;9(11):e111592.

109. Wang H, Song X, Huang Q, et al. LGALS3 promotes treatment resistance in glioblastoma and is associated with tumor risk and prognosis. *Cancer Epidemiol Biomarkers Prevent: Publ Am Assoc Cancer Res Cosponsored Am Soc Prevent Oncol*. 2019;28(4): 760-769.

110. Binh NH, Satoh K, Kobayashi K, et al. Galectin-3 in preneoplastic lesions of glioma. *J Neuro-Oncol*. 2013;111(2):123-132.

111. Thomas L, Pasquini LA. Galectin-3-mediated glial crosstalk drives oligodendrocyte differentiation and (re)myelination. *Front Cell Neurosci*. 2018;12:297.

112. Reichert F, Rotshenker S. Galectin-3 (MAC-2) controls microglia phenotype whether amoeboid and phagocytic or branched and non-phagocytic by regulating the cytoskeleton. *Front Cell Neurosci*. 2019; 13:90.

113. Piao Y, Henry V, Tiao N, et al. Targeting intercellular adhesion molecule-1 prolongs survival in mice bearing bevacizumab-resistant glioblastoma. *Oncotarget*. 2017;8(57):96970-96983.

114. Lin JC, Tsai JT, Chao TY, Ma HI, Liu WH. Musashi-1 enhances glioblastoma migration by promoting ICAM1 translation. *Neoplasia*. 2019;21(5):459-468.

115. Bui TM, Wiesolek HL, Sumagin R. ICAM-1: a master regulator of cellular responses in inflammation, injury resolution, and tumorigenesis. *J Leukoc Biol*. 2020;108(3):787-799.

116. Qian J, Wang C, Wang B, et al. The IFN-gamma/PD-L1 axis between T cells and tumor microenvironment: hints for glioma anti-PD-1/PD-L1 therapy. *J Neuroinflammation*. 2018;15(1):290.

117. Noman MZ, Desantis G, Janji B, et al. PD-L1 is a novel direct target of HIF-1alpha, and its blockade under hypoxia enhanced MDSC-mediated T cell activation. *J Exp Med*. 2014;211(5): 781-790.

118. Lamano JB, Lamano JB, Li YD, et al. Glioblastoma-derived IL6 induces immunosuppressive peripheral myeloid cell PD-L1 and promotes tumor growth. *Clin Cancer Res: Off J Am Assoc Cancer Res*. 2019;25(12):3643-3657.

119. Saidi A, Hagedorn M, Allain N, et al. Combined targeting of interleukin-6 and vascular endothelial growth factor potently inhibits glioma growth and invasiveness. *Int J Cancer*. 2009;125(5): 1054-1064.

120. Lim M, Xia Y, Bettegowda C, Weller M. Current state of immunotherapy for glioblastoma. *Nat Rev Clin Oncol*. 2018;15(7):422-442.

121. Wei J, Chen P, Gupta P, et al. Immune biology of glioma-associated macrophages and microglia: functional and therapeutic implications. *Neuro-Oncology*. 2020;22(2):180-194.

122. Grégoire H, Roncali L, Rousseau A, et al. Targeting tumor associated macrophages to overcome conventional treatment resistance in glioblastoma. *Front Pharmacol*. 2020;11:368.

123. Flores-Toro JA, Luo D, Gopinath A, et al. CCR2 inhibition reduces tumor myeloid cells and unmasks a checkpoint inhibitor effect to slow progression of resistant murine gliomas. *Proc Natl Acad Sci U S A*. 2020;117(2):1129-1138.

124. Brandenburg S, Muller A, Turkowski K, et al. Resident microglia rather than peripheral macrophages promote vascularization in brain tumors and are source of alternative pro-angiogenic factors. *Acta Neuropathol*. 2015;131(3):365-378.

125. Angara K, Borin TF, Rashid MH, et al. CXCR2-expressing tumor cells drive vascular mimicry in antiangiogenic therapy-resistant glioblastoma. *Neoplasia*. 2018;20(10):1070-1082.

126. Yan D, Kowal J, Akkari L, et al. Inhibition of colony stimulating factor-1 receptor abrogates microenvironment-mediated therapeutic resistance in gliomas. *Oncogene*. 2017;36(43):6049-6058.

127. Pyonteck SM, Akkari L, Schuhmacher AJ, et al. CSF-1R inhibition alters macrophage polarization and blocks glioma progression. *Nat Med*. 2013;19(10):1264-1272.

128. Butowski N, Colman H, De Groot JF, et al. Orally administered colony stimulating factor 1 receptor inhibitor PLX3397 in recurrent glioblastoma: an Ivy Foundation Early Phase Clinical Trials Consortium phase II study. *Neuro-Oncology*. 2015;18(4):557-564.

129. Zhan L, Krabbe G, Du F, et al. Proximal recolonization by self-renewing microglia re-establishes microglial homeostasis in the adult mouse brain. *PLoS Biol*. 2019;17(2):e3000134.

130. Quail DF, Bowman RL, Akkari L, et al. The tumor microenvironment underlies acquired resistance to CSF-1R inhibition in gliomas. *Science*. 2016;352:aad3018.

SUPPORTING INFORMATION

Additional supporting information may be found in the online version of the article at the publisher's website.